ACS OMEGA

Open Access

http://pubs.acs.org/journal/acsodf

Article

Mercury Can Bond to α-Carbon of Curcumin Increasing Stability in Aqueous Medium and Demonstrated Selective Cytotoxicity against Acute Leukemia

Sougata Mondal,[#] Upasana Das,[#] Oyendrila Ghosh, Bidisha Maiti, Shuvam Halder, Uttam Pal, Kalyan Kusum Mukherjee, and Supratim Ghosh*

Cite This: *ACS Omega* 2025, 10, 17416−17434

Read Online

ACCESS | Metrics & More | Article Recommendations | Supporting Information

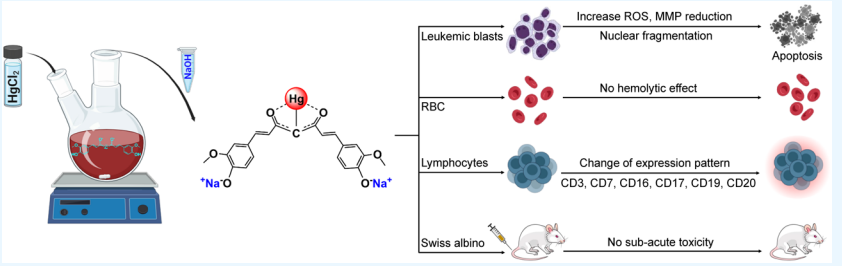

ABSTRACT: Natural products ranging from phytochemicals to metals are well-known for their therapeutic benefits on different cancer types, including acute leukemia. However, bioavailability significantly limited the applications of various polyphenolic molecules, such as curcumin, while toxicity challenged the medicinal applications of heavy metals, such as mercury (Hg). Specifically, in case of curcumin derivatives, simultaneous solubility, stability, and bioactivity in the aqueous medium remain unachieved, leading to poor clinical translation. We demonstrate for the first time that the above-mentioned challenges could be resolved by covalently bonding mercury to the α-carbon of curcumin. The resultant organomercury compound ((1E,6E)-1,7-bis(4-hydroxy-3-methoxyphenyl)-3,5-dioxohepta-1,6-dien-4-yl)mercury or α-Mercurin is soluble in alkaline conditions and remains stable for at least 24 h. Cell viability assays demonstrated selective cytotoxicity of α-Mercurin against acute leukemia cells, compared to healthy human peripheral blood mononuclear cells, in vitro. Experimental IC_{50} on MOLT-4 and HL-60 cells remained in the lower micromolar range, and potential mode of action includes apoptosis. Ex vivo analysis also demonstrated that α-Mercurin can eliminate immature blasts from acute lymphoblastic leukemia patients' blood samples and also enhance expression of immune markers, with no notable toxicity on red blood cells as well as lymphocytes. Finally, intravenous administration of α-Mercurin showed no subacute toxicity, in vivo.

INTRODUCTION

Polyphenols and other natural products, including heavy metals and metalloids established their importance in the field of cancer therapy for long.[1−4] Yet, clinical use of many potent candidates, like curcumin is still remaining as a challenge due to poor bioavailability,[5,6] while application of mercury suffers from its toxicity.[7,8] Curcumin is popularly known for its immunomodulating property[9−11] as well as antiproliferative activity against different cancer types,[12−14] including hematological malignancies.[15−17] However, its poor absorption from the intestine upon oral administration,[18,19] and unsuitability for intravenous delivery due to hydrophobic nature, significantly limited its biomedical applications. Furthermore, rapid decomposition of curcumin at alkaline conditions (pH ≥ 7.2) in the aqueous medium also limited its prospect.[20] In order to achieve an improved pharmacological profile, several research groups tried different strategies to form chemical analogs.[21−24] Numerous researchers tried nano-formulation[25,26] and metal complexation[27,28] for solubilizing curcumin in aqueous environment, without significantly distorting its structure as well as biological activity. Nano-formulations suffered from poor biodistribution,[29] while metal complexes for their inability to achieve simultaneous solubility, stability, and bioactivity in the cellular environment. In all cases, chelate-type metal complexes were formed utilizing the β-diketo moiety[30−33] as Lewis acid, leaving the acidic α-carbon unprotected. This acidic α-carbon can act as a potent nucleophile and could be attacked by cations or electrophiles, especially at higher pH in the aqueous environment.

Received: November 25, 2024
Revised: March 8, 2025
Accepted: March 12, 2025
Published: April 24, 2025

Scheme 1. Reaction Scheme for the Synthesis of α-Mercurin. (a) Curcumin, (b) Curcumin in the Carbanion Form (Intermediate), (c) α-Mercurin, and (d) α-Mercurin in Aqueous NaOH

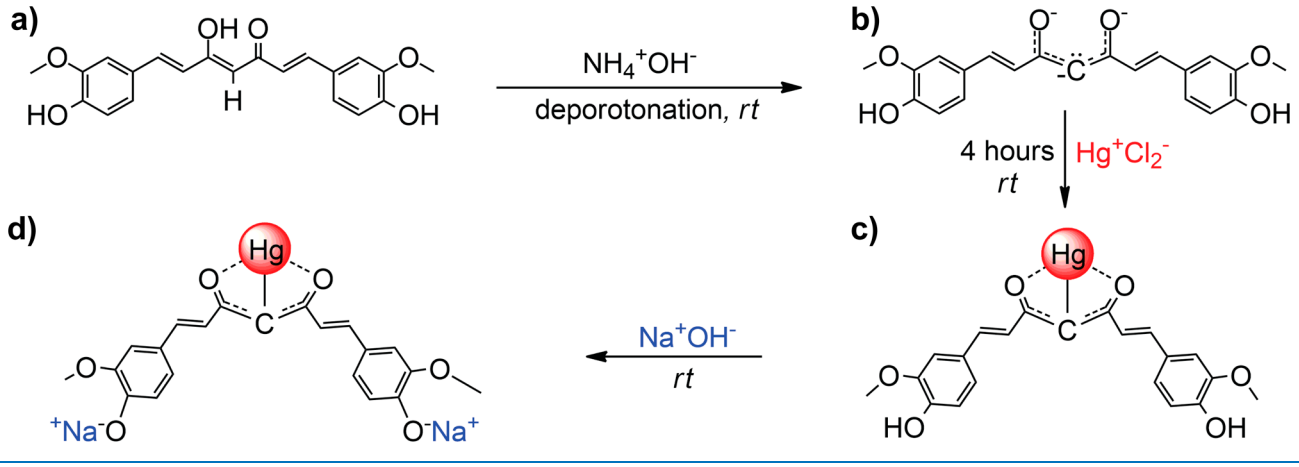

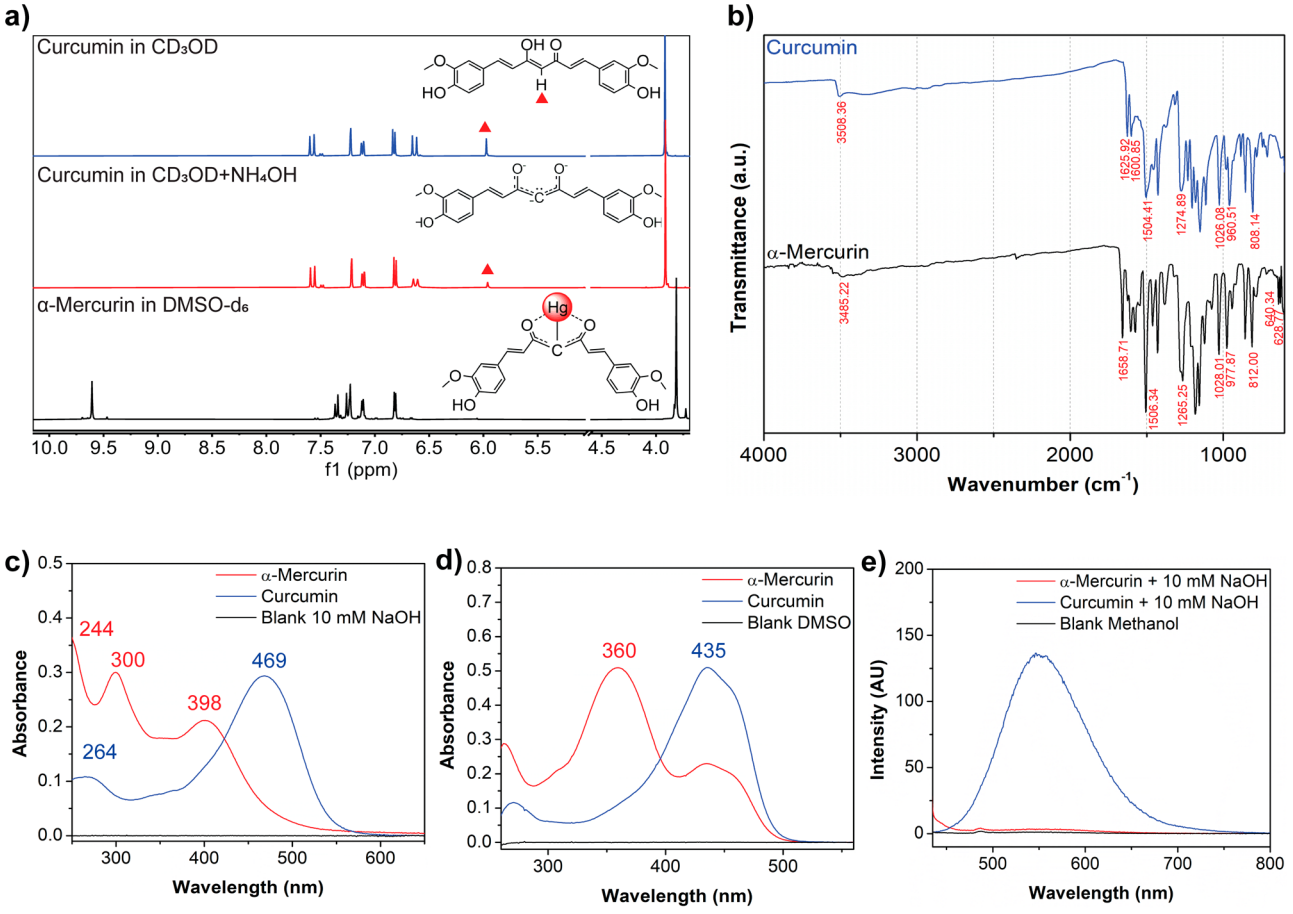

Figure 1. (a) ^{1}H NMR spectrum of curcumin in CD_3OD (top panel) showing its characteristic pattern, including the band at 5.96 ppm for hydrogen associated with α-carbon. Addition of NH_4OH resulted to significant reduction (~70% reduction) in ^{1}H peak intensity at 5.96 ppm, suggesting displacement of hydrogen from α-carbon, marked by red triangles (middle panel). ^{1}H NMR spectra were recorded 5 min following sample preparation. α-Mercurin is insoluble in CD_3OD; therefore, corresponding NMR spectra are recorded in DMSO-d_6 (bottom panel). ^{1}H NMR spectrum of α-Mercurin shows the absence of peak at 5.96 ppm, suggesting no hydrogen atom is associated with the α-carbon. (b) Comparative FTIR spectra of α-Mercurin and curcumin. Three new intense peaks at 1658.71, 640.34, and 628.77 cm^{-1} appeared in the spectrum of α-Mercurin, corresponding to keto/carbonyl ν(C═O), metal−carbon and metal−oxygen stretching or bending vibrations, respectively. (c) Comparative UV−visible spectra of α-Mercurin and curcumin in aqueous 10 mM NaOH. Absorbance of curcumin at 469 and 264 nm are shifted to higher energy fields at 398 and 244 nm, respectively, in α-Mercurin. A new peak appeared for α-Mercurin at 300 nm. (d) Comparative UV−visible spectra of α-Mercurin and curcumin in DMSO showing a decrease in absorbance of curcumin at 435 nm due to bonding with mercury. A new peak appeared in the spectrum of α-Mercurin at 360 nm. (e) Comparative fluorescence spectra of α-Mercurin and curcumin with fluorescence excitation at 426 nm. Samples were solubilized in aqueous 10 mM NaOH and further diluted in Methanol before recording the emission spectra. Emission maxima of curcumin ~ 550 nm were quenched completely after bonding with Mercury (Hg).

https://doi.org/10.1021/acsomega.4c10710
ACS Omega 2025, 10, 17416−17434

Acute malignancies of lymphoid as well as myeloid progenitor cells are important challenges across the globe.[34−37] The prevalence of this disease is increasing worldwide, with modern lifestyle.[38] Currently used treatment modalities including combination chemotherapy with cytarabine (cytosine arabinoside; Ara-C), vincristine, and anthracyclines (e.g., daunorubicin, idarubicin) cause severe myelosuppression, neurotoxicity, cardio, and hepatocellular toxicities.[39−44] Additionally, bone marrow can expand due to the accumulation of immature blasts, leading to severe bone and joint pain.[45] Adverse effects of the present therapeutics prompted for improved drug candidates with novel mechanism of action. Derivatives of heavy metals and metalloids are well-known for their versatile biomedical benefits.[46] Old medicinal systems[47] like *Siddha* successfully used formulations of mercury and arsenic for the treatment of hematological disorders.[48−52] However, the toxic effects of mercury have severely limited its application in modern medicine. In contrast, a recent study published by Kannan et al. revealed the cytotoxic effect of mercury-based formulations against cancer cells, in vitro and in vivo.[53] Mercury at varying concentrations can also enhance hematopoietic stem cell differentiation.[54] Such promising activities of mercury may lead to novel and efficacious therapeutics, if bonded with a suitable organic moiety and administered in appropriate doses, via a suitable route.

In the present work, we demonstrate for the first time that mercury could be bonded to the α-carbon atom of curcumin via coordinate covalent bonding, and the resultant organomercury compound, named as α-Mercurin, is simultaneously soluble and stable in aqueous medium at alkaline condition. The synthesized compound α-Mercurin showed selective cytotoxicity toward acute leukemia cells (MOLT-4 and HL-60), compared to healthy human peripheral blood mononuclear cells (PBMCs) in cell culture. Further in vitro investigations showed that α-Mercurin treatment increased intracellular reactive oxygen species (ROS) levels, causing nuclear fragmentation and reduced mitochondrial transmembrane potential (MMP), leading to apoptosis. α-Mercurin also demonstrated its therapeutic potential by selectively eliminating immature leukemic blasts from acute lymphoblastic leukemia (ALL) patients' blood samples, without any deleterious effect on healthy lymphocytes and red blood cells (RBC). Furthermore, α-Mercurin also showed immunomodulating properties by changing the expression of different Cluster of Differentiation (CD) molecules (CD3, CD7, CD16, CD17, CD19, CD20, and CD14), ex vivo. Preliminary toxicity studies on Swiss albino mice demonstrated that intravenous administration with a dose of ∼3.3 mg/kg body weight, twice a week for 8 weeks, showed no subacute toxicity in terms of behavioral and hematological parameters, in vivo.

RESULTS AND DISCUSSION

Synthesis. The novel organomercury compound, α-Mercurin, having [IUPAC name: ((1E,6E)-1,7-bis(4-hydroxy-3-methoxyphenyl)-3,5-dioxohepta-1,6-dien-4-yl)mercury] general formula $C_{21}H_{18}O_6Hg$, was synthesized by reacting mercury(II) chloride ($HgCl_2$) with curcumin ($C_{21}H_{20}O_6$) in ethanol: water mixture 95:5 (v/v), at pH 8.2−8.4 for 4 h at room temperature (∼25 °C) (Scheme 1). The synthesized compound was further washed with ethanol and water to remove unreacted curcumin and mercury, then the final product was obtained with a purity >95%. Further, α-Mercurin was resuspended in DMSO or aqueous 10 mM NaOH solution, depending upon experimental requirements. The stepwise reaction mechanism was investigated by using ^{1}H NMR spectroscopy (Figure 1a). Results obtained by EDAX analysis (Supporting Information Figure S1) suggested the elemental ratio in the compound, while HR-MS (Supporting Information Figure S2) and ESI−MS (Supporting Information Figure S3) spectra confirmed the mass. Elemental analysis suggested mercury content is 36.1% by weight. Therefore, in the future, α-Mercurin could be applied clinically with a dose of ∼5.5 μg/kg body weight/day, following WHO guidelines.[55] Complete structural characterization of the synthesized organomercury compound was done by UV−visible, fluorescence, FT-IR, XPS (C 1s, O 1s, Hg 4f, Hg 4d), and NMR (^{1}H, ^{13}C, DEPT, 2D-NMR, solid-state NMR) spectroscopy.

Spectroscopic Characterizations. The FT-IR spectra of α-Mercurin showed significant changes compared to that of curcumin (Figure 1b). The low-intensity broad band at 3485.22 cm^{-1} indicates phenolic ν(O−H) stretching vibration,[56] while enolic δ(O−H) bending vibrations of curcumin, attributed to the band at 1625.92 cm^{-1}, is no longer present in the FT-IR spectrum of α-Mercurin, indicating the absence of the enolic form in the synthesized compound. The transmittance band for stretching vibration of ν(C═O) at 1429.19 cm^{-1} became intensified upon mercury bonding, while a newly identified strong peak at 1658.71 cm^{-1} in the spectrum of α-Mercurin also could be attributed to ν(C═O) stretching vibration, suggesting predominance of the β-diketo form in the synthesized compound. The new pronounced bands at 640.34 and 628.77 cm^{-1} could be attributed to a mixture of metal−carbon and metal−oxygen stretching or bending vibrations in α-Mercurin, indicating the simultaneous interaction of mercury with carbon as well as oxygen.

The comparative UV−visible spectra in 10 mM NaOH solution (Figure 1c), suggested that the absorbance of curcumin at 469 and 264 nm for $\pi \rightarrow \pi^*$ and $n \rightarrow \pi^*$ transitions is shifted to higher energy field at 398 and 244 nm, respectively. The interaction with mercury also caused appearance of a new peak at 300 nm. Spectra in DMSO showed a significant decrease in absorbance at 435 nm due to bonding with mercury, including appearance of a new peak at 360 nm (Figure 1d). Fluorescence spectra showed significant quenching in emission at ∼550 nm (Figure 1e) after mercury binding.

Computational Analysis. To understand the stepwise reaction mechanism, Density Functional Theory (DFT) calculations were performed. Findings suggested that the reaction is initiated by displacing hydrogen ions (H^+) consecutively from the β-enol group and α-carbon of curcumin molecule, which is also observed in the ^{1}H NMR spectrum (solvent: CD_3OD) showing a significant reduction in peak intensity at 5.96 ppm after addition of NH_4OH (Figure 1a); the peak at 5.96 ppm is assigned to the proton associated with the α-carbon. The said deprotonation resulted to a reaction intermediate, α-carbanion (Scheme 1b), having a pair of unshared electrons. In the following step, α-carbanion further shares its electron pair with the unoccupied s-orbital of mercury ion (Hg^{2+}), forming a stable coordinate covalent bond by overlapping carbon-p and mercury-s orbitals. The product is further stabilized by distal coordination between mercury and oxygen atoms of β-diketo groups along with water molecules in aqueous environment. Natural population analysis (NPA) for atomic contributions suggested overlapping of mercury-s and

https://doi.org/10.1021/acsomega.4c10710
ACS Omega 2025, 10, 17416−17434

a)

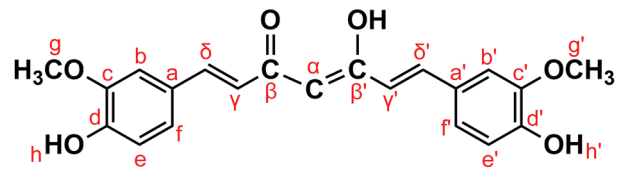

b)

Bonds	Bond length in Angstrom (Å)	
	Curcumin	α-Mercurin
$C_\alpha - C_\beta$	1.436	1.409
$C_\alpha - C_{\beta'}$	1.383	1.409
$C_\beta - O$	1.261	1.268
$C_{\beta'} - O$	1.325	1.269

c)

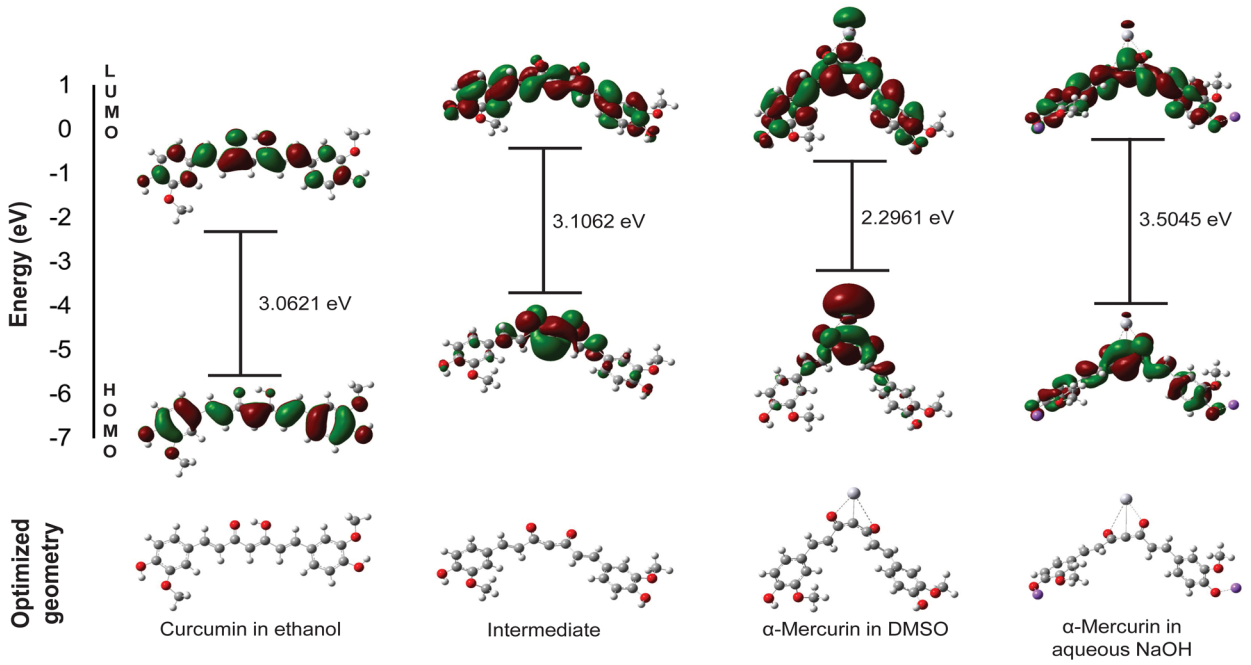

Figure 2. (a) Depiction of α, β, and γ-carbons as referred in the present study. (b) Difference in bond lengths of optimized geometries for curcumin and α-Mercurin, as calculated from DFT analysis. (c) Comparison of DFT-optimized geometries along with HOMO−LUMO energy gap of curcumin, intermediate (curcumin in the α-carbanion form), and α-Mercurin in DMSO and aqueous NaOH.

oxygen-p orbitals at the bridge region (Supporting Information Table S1). Ab Initio calculations also suggested that binding of mercury made significant changes in the bond lengths as well as bond orders at the ethylene bridge region (Figure 2b). The bond length between oxygen atoms of diketo groups and C_β /$C_{\beta'}$ increased due to metal interaction, compared to the keto group (C═O) of curcumin, while the bond lengths between C_α and C_β /$C_{\beta'}$ exhibited a length of 1.409 Å which is shorter than C−C length and longer than C═C length, representing an intermediate bond order. The calculated Hg−C_α bond length in α-Mercurin is 2.361 Å, which is slightly higher than the Hg-carbon bond length reported for other organomercury compounds,[57,58] indicating the predominant coordinate covalent character of the corresponding bond. However, oxygen atoms of β-diketo groups are at a distance of ∼3.35 Å from the mercury atom, which is ∼1 Å more than the length of mercury−oxygen covalent bond and almost similar to the sum of the van der Waals radii of oxygen and mercury atoms. The distance between oxygen and mercury indicates their distal coordination,[59] supporting the stability of the synthesized compound. Investigation of frontier molecular orbitals, highest occupied molecular orbital (HOMO), and lowest unoccupied molecular orbital (LUMO) revealed changes in electron-density distribution across the π-conjugated system of curcumin upon mercury bonding. The displacement of H^+ ion from α-carbon of curcumin caused localization of the largest electron density of HOMO around the bridge region, especially on α-carbon (Figure 2c). This localized electron density then attracted the electrophile, Hg^{2+}, for reaction and bond formation; findings are also in agreement with those from the NMR study (Figure 1a).

Stability in Aqueous Medium. α-Mercurin is soluble in aqueous medium, in presence of 10 mM NaOH (≤2 mg/mL), and it is also highly soluble in DMSO, DMF (≥50 mg/mL). The stability of α-Mercurin in 10 mM NaOH at aqueous environment was investigated for 24 h, using ^{1}H NMR spectroscopy at 298 K. Results showed no significant changes in the spectra (Figure 3a), indicating notable stability in aqueous medium, even at pH ∼ 8.5. The stability was further investigated in alkaline aqueous solution. UV−visible spectra were recorded at an interval of 4 h for 24 h by dissolving the compound in 10 mM NaOH. Further, mass spectra were also acquired after incubation for 24 h compared to 0 h at similar conditions. Both the UV−visible (Figure 3b) and mass spectra (Supporting Information Figure S3) suggested that the compound is stable in aqueous medium, even at alkaline conditions, unlike curcumin.

The stability of α-Mercurin was also investigated at physiological pH, using UV−visible spectroscopy. α-Mercurin was dissolved in aqueous 10 mM NaOH and further diluted in 10 mM phosphate buffer of pH 7.2 and 6.5. At pH 7.2, no significant changes in the spectra (Figure 3c) were observed suggesting that the compound is stable in physiological pH. However, at pH 6.5 the data showed a gradual reduction in absorbance, starting from 4 h (Supporting Information Figure S4). Furthermore, stability of α-Mercurin in presence of

https://doi.org/10.1021/acsomega.4c10710
ACS Omega 2025, 10, 17416−17434

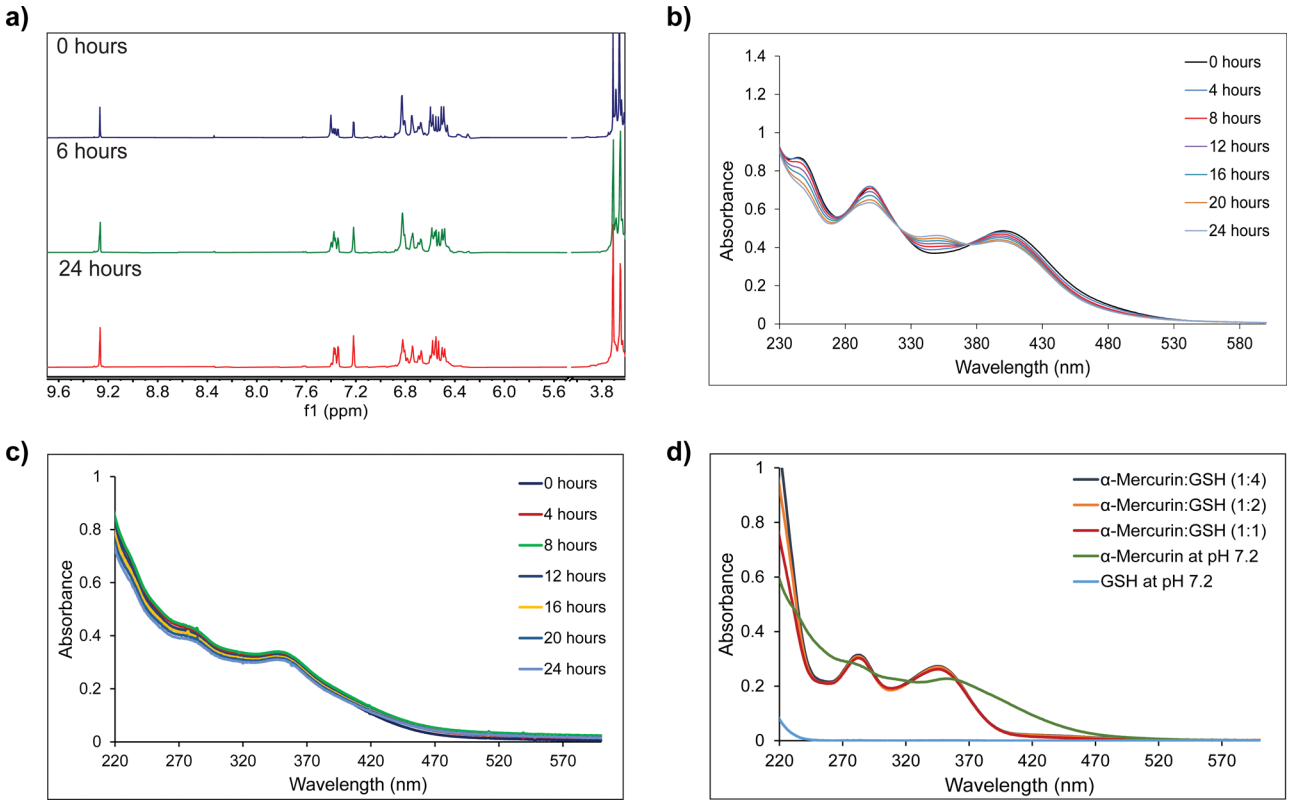

Figure 3. (a) For biological applications α-Mercurin was solubilized in aqueous 10 mM NaOH and stability was investigated by ^{1}H NMR spectroscopy. Spectra were recorded by dissolving α-Mercurin in D_2O containing 10 mM NaOH (pH ~ 8.5) at 0, 6, and 24 h, showing no significant changes in the spectral pattern, which demonstrates α-Mercurin is stable in aqueous medium at alkaline conditions for at least 24 h. (b) Stability of the compound in aqueous 10 mM NaOH was investigated by UV−visible spectroscopy. Spectra were recorded at an interval of 4 h for 24 h, suggesting no significant changes in the spectral pattern, that also demonstrates α-Mercurin is stable in aqueous medium at alkaline condition for at least 24 h. (c) Stability of the compound at physiological pH (pH = 7.2) was investigated by UV−visible spectroscopy. α-Mercurin was dissolved in aqueous 10 mM NaOH (pH ~ 8.5) and further diluted in 10 mM phosphate buffer (pH = 7.2) and spectra were recorded at an interval of 4 h for 24 h, suggesting no significant changes in the spectral pattern, demonstrating stability of α-Mercurin at pH = 7.2. (d) Stability of α-Mercurin in presence of reduced glutathione (GSH) was investigated by UV−visible spectroscopy. α-Mercurin was dissolved in aqueous 10 mM NaOH (pH ~ 8.5) and diluted in 10 mM phosphate buffer (pH = 7.2). Further, GSH was added at the molar ratio of α-Mercurin: GSH = 1:1, 1:2 and 1:4; incubated in dark for 4 h. Spectral patterns remain similar in presence as well as in absence of GSH, suggesting α-Mercurin is stable in the presence of GSH.

endogenous metal ion Fe(III) was investigated. UV−visible spectra suggested no significant changes, while X-ray photoemission demonstrated a stable Hg−C bond even in the presence of Fe(III) (Supporting Information Figure S5). To investigate the possible interaction of α-Mercurin with sulfur (S) atom from cellular reduced glutathione (GSH), the compound was incubated with GSH in a phosphate buffer of pH 7.2 and investigated with UV−visible spectroscopy. The corresponding data (Figure 3d) suggested that the compound is stable in presence of GSH. Therefore, α-Mercurin demonstrated significant stability in an aqueous solution, in the presence of relevant biological factors, suggesting its suitability for biomedical applications.

Chemical Structure. α-Mercurin was further characterized with ^{13}C NMR spectroscopy (solvent: DMSO-d_6), compared to curcumin[60,61] (Supporting Information Figure S6 and S7). The ^{13}C signal at 101.01 ppm of curcumin that is assigned to α-carbon is shifted upfield by δ 4.62 to 96.39 ppm, upon compound formation. The said upfield shift could be explained by the shielding effect resulted from the accumulated electron density around the α-carbon; similar observations are also found in the charge distribution analysis of DFT calculations (Figure 4b). The increment in electron density surrounding the α-carbon in the compound created an electron pull, causing electron cloud shift from the β-carbons as well as γ-carbons, leading to a deshielding effect. The said effect is observed in the corresponding ^{13}C NMR resonances; assigned bands of β-carbon and γ-carbon shifted downfield from 183.33 and 121.20 to 194.73 and 124.59 ppm, respectively (Figure 4c). The observation is also consistent with ^{13}C CP/MAS solid-state NMR (ssNMR) spectra (Figure 4d), where the α, β and γ-carbons of curcumin resonating at 98.95, 182.76/187.36 and 122.41/123.21 ppm[62] shifted to 89.67, 191.86/196.09 and 123.87 ppm, respectively in α-Mercurin (Supporting Information Figure S8). ^{13}C DEPT experiments (DEPT-45, DEPT-90, and DEPT-135) in DMSO-d_6 confirmed the number of hydrogens associated with different carbon atoms (Supporting Information Figure S9).

^{1}H ssNMR spectra obtained under MAS condition (Supporting Information Figure S10) showed a band at 17.43 ppm for the enolic proton of curcumin[63] is no longer present in α-Mercurin, indicating prevalence of β-diketo form upon mercury bonding, which is also in accordance with the findings from IR spectrum. The said observation is also in agreement with the ^{1}H NMR spectra of α-Mercurin (solvent: DMSO-d_6) showing the absence of peak at 16.39 ppm, which

https://doi.org/10.1021/acsomega.4c10710
ACS Omega 2025, 10, 17416−17434

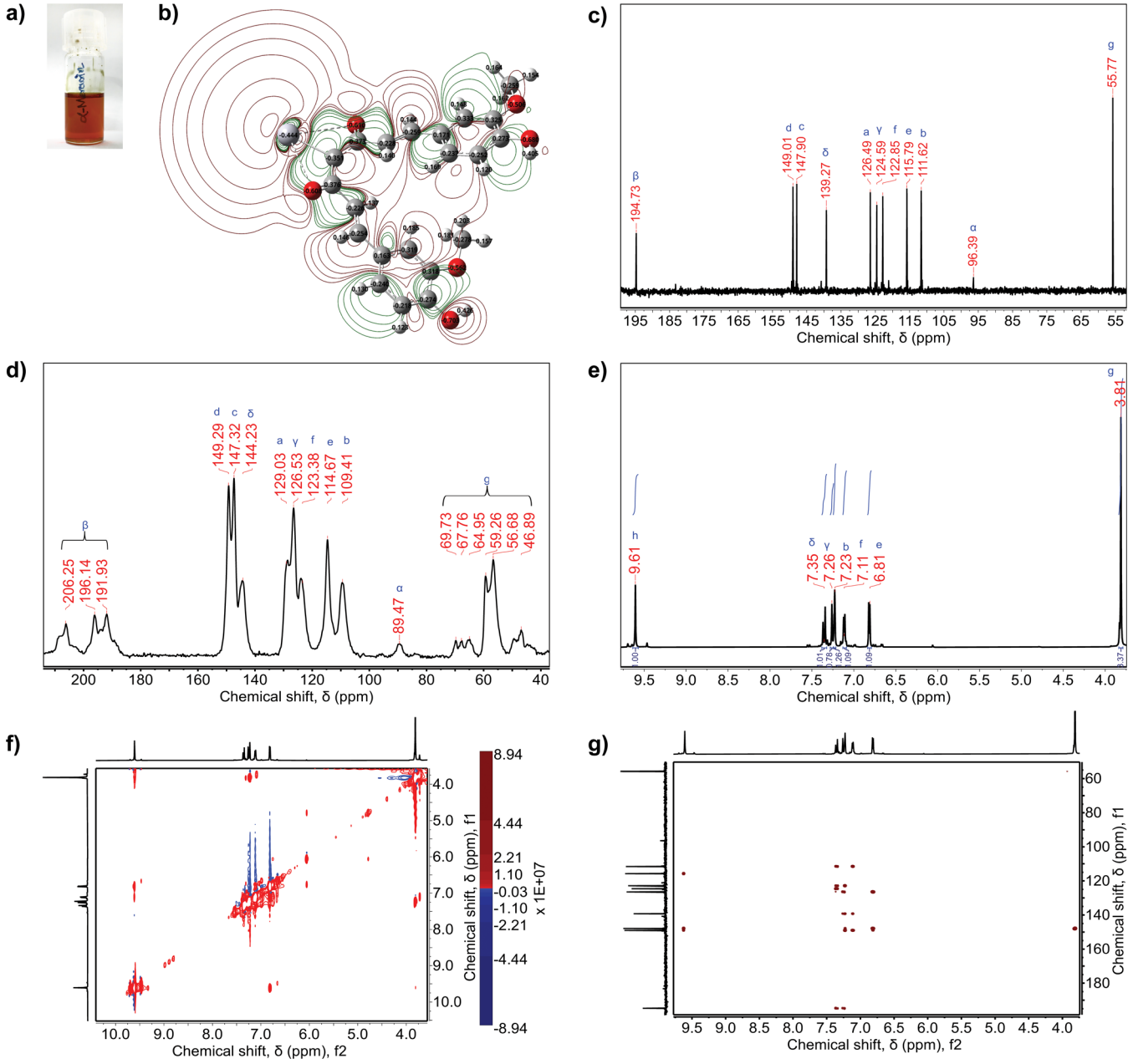

Figure 4. (a) Physical appearance of α-Mercurin dissolved in DMSO. (b) Charge distribution and contour plot of electron densities around the atoms of the synthesized compound suggested by in silico analysis. Red lines represent positive contour, while green lines represent negative contour. (c) ^{13}C NMR spectra of α-Mercurin dissolved in DMSO-d_6, showing peaks of corresponding carbons referred in labeled optimized geometry. The bands at 55.77, 96.39, and 194.73 ppm correspond to methoxy ($-OCH_3$) carbons, α-carbon and β-carbons; respectively. (d) ^{13}C CP/MAS solid state NMR spectra of α-Mercurin, showing peaks of corresponding carbons referred in labeled optimized geometry. The multiplet at 46.89−69.73 ppm and the triplet at 191.93−206.25 ppm, are assigned to methoxy ($-OCH_3$) carbons and β-carbons, respectively. The band at 89.47 ppm corresponds to the α-carbon. The data suggest similar spectral pattern with ^{13}C NMR spectra acquired in DMSO-d_6. (e) ^{1}H NMR spectra of α-Mercurin dissolved in DMSO-d_6, showing peaks of corresponding protons referred in labeled optimized geometry. The ^{1}H peaks at 3.81 and 9.61 ppm correspond to methoxy ($-OCH_3$) protons and phenoilc ($-OH$) protons, respectively. (f) ^{1}H−^{1}H (f1/f2) NOESY spectrum of α-Mercurin in DMSO-d_6. Red contours represent positive crosspeaks, while blue contours represent negative crosspeaks. (g) ^{13}C−^{1}H (f1/f2) HMBC spectra of α-Mercurin in DMSO-d_6, suggesting distant correlation of protons and carbons, corresponding to three-dimensional geometry of α-Mercurin in DMSO.

is assigned to the β-enol proton (Supporting Information Figure S11). ^{1}H associated with the α-carbon of curcumin, resonating at 6.06 ppm, is missing in α-Mercurin, indicating its displacement, supporting the mentioned reaction mechanism.

The conjugated ^{1}H signals in the region of 6.75−7.55 ppm of curcumin could be assigned to aromatic and heptadiene chain protons. In case of α-Mercurin, this region became more clustered and resonates in the region of 6.81−7.35 ppm, due to change in electron distribution for mercury binding. Within this cluster, only the protons resonated at 6.75 ppm for curcumin experienced a downfield shift by δ 0.51 ppm in α-Mercurin; said resonance could be assigned to the protons attached to γ-carbons (Figure 4e). This shift occurred due to the electronic deshielding as a result of electron pull toward α-

https://doi.org/10.1021/acsomega.4c10710
ACS Omega 2025, 10, 17416−17434

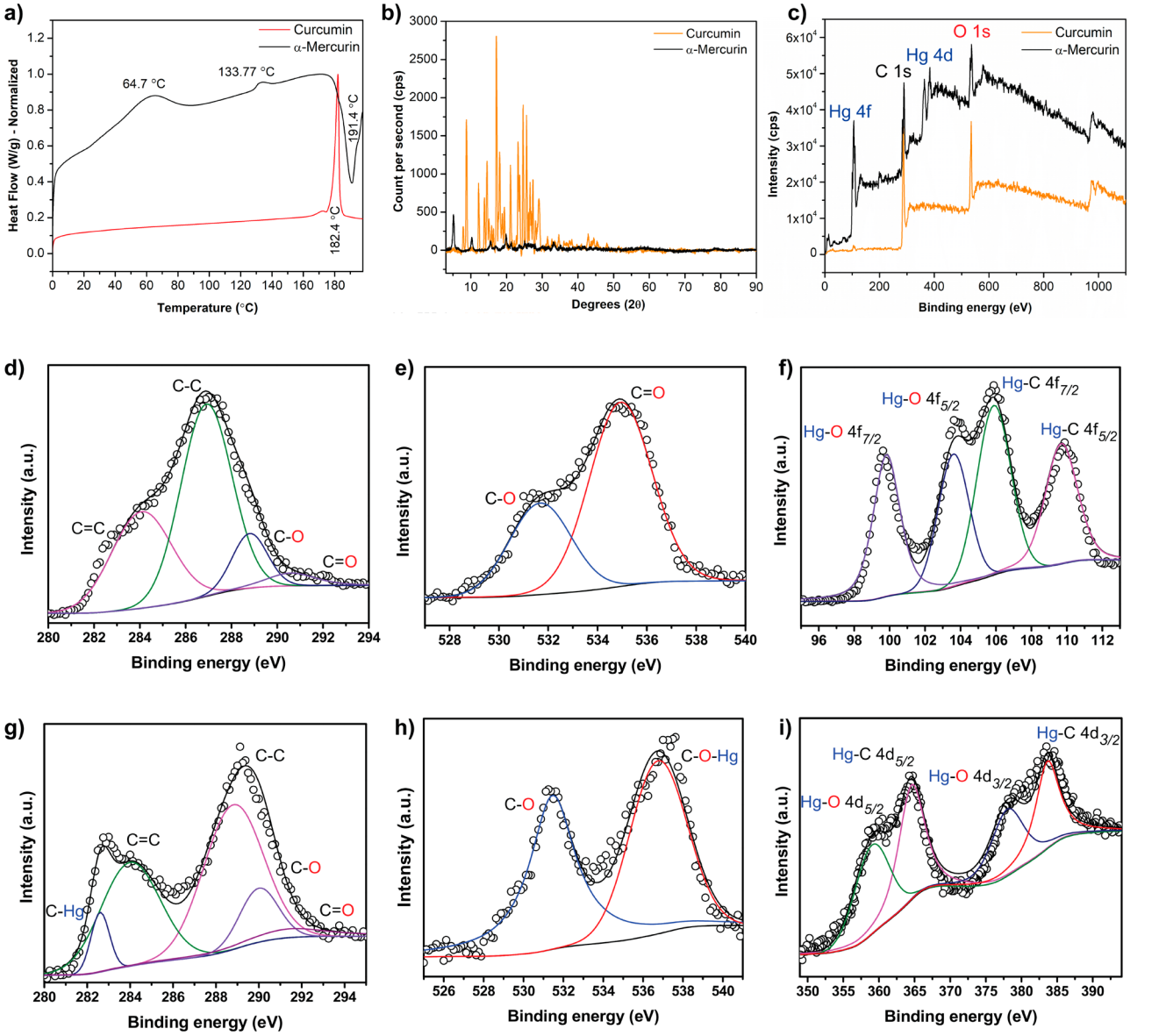

Figure 5. (a) Comparative DSC thermogram of α-Mercurin suggests endothermic and exothermic transitions, while thermogram of curcumin showing a single endothermic peak. (b) Comparative Powder XRD spectra suggests no characteristic Bragg peaks of curcumin appears in the α-Mercurin spectrum, indicating formation of amorphous structure. (c) Comparative XPS survey scan suggests, in comparison to curcumin, two new peaks appear in α-Mercurin spectrum, correspond to Hg for 4f and 4d core-level electrons. (d) Deconvoluted XPS spectra of C 1s core-level electrons of curcumin suggests four components for sp^2 carbon, sp^3 carbon, C−O and C═O. (e) Deconvoluted XPS spectra of O 1s core-level electrons of curcumin suggests two components for C−O and C═O environments. (f) Deconvoluted XPS spectra of Hg 4f core-level electrons of α-Mercurin suggests presence of four components, with B_E of 99.8 and 103.69 eV for Hg···O $4f_{7/2}$ and $4f_{5/2}$ photoemission while photoemissions at 105.94 and 109.84 eV correspond to Hg−C $4f_{7/2}$ and $4f_{5/2}$ environments. (g) Deconvoluted XPS spectra of C 1s core-level electrons of α-Mercurin suggesting five components for sp^2 carbon, sp^3 carbon, C−O and C═O along with a new peak at 282.59 eV that is attributable to C−Hg photoemission. (h) Deconvoluted XPS spectra of O 1s core-level electrons of α-Mercurin suggests two components for C−O and C═O···Hg environments. (i) Deconvolution of XPS spectra of Hg 4d core-level electrons of α-Mercurin suggests presence of four components, with B_E 359.6 and 378.47 eV for Hg···O $4d_{5/2}$ and $4d_{3/2}$ photoemission while the photoemissions at 364.73 and 383.89 eV correspond to Hg−C $4d_{5/2}$ and $4d_{3/2}$ environments.

carbon, the observation is consistent with the ^{13}C NMR spectra.

Further, the structural conformation of α-Mercurin was studied using 2D $^1H-^1H$ (f1/f2) Nuclear Overhauser effect spectroscopy (NOESY), $^{13}C-^1H$ (f1/f2) heteronuclear multiple bond correlation (HMBC), and $^{13}C-^1H$ (f1/f2) heteronuclear single quantum coherence (HSQC) spectroscopy. A pronounced NOESY cross peak was observed between resonances 3.81(f1)/7.23(f2) ppm for interaction of methoxy proton with an adjacent proton from the aromatic ring (Figure 4f); another NOESY cross peak was observed at 6.81(f1)/7.11(f2) ppm for interaction between two adjacent protons of the aromatic ring. NOESY cross peak for interaction between the protons of ethylene chain and aromatic rings was observed between resonances 7.35(f1)/7.11(f2) ppm. The structure of α-Mercurin was further verified with $^{13}C-^1H$ correlation by HMBC spectroscopy (Figure 4g). A cross peak at 149.01(f1)/3.81(f2) ppm was observed for interaction between the

https://doi.org/10.1021/acsomega.4c10710
ACS Omega 2025, 10, 17416−17434

methoxy proton and phenolic−OH associated carbon, while cross peaks for phenolic proton and aromatic ring carbons were observed at 115.79(f1), 147.90(f1), 149.01(f1)/9.61(f2) ppm. To investigate the proton-carbon single bond correlation of the compound, HSQC was performed (Supporting Information Figure S12), the cross peak at 55.77(f1)/3.81(f2) ppm corresponds to the C−H single bond of the methoxy group, while the cross-peaks in the region of 111.62(f1) −139.27(f1)/6.81(f2)−7.35(f2) ppm were from C−H single bonds of aromatic ring and heptadiene chain. However, no HSQC cross-peaks were observed at 194.73 as well as 9.61 ppm, assigned to β carbons and phenolic protons, respectively. Displacement of hydrogen (H^+) from α-carbon was further reconfirmed by the absence of crosspeak at 96.39 ppm (^{13}C), assigned to the α-carbon. Therefore, observed cross-peaks in 2D-NMR spectroscopy clearly suggested simultaneous bonding of mercury with α-carbon and distal interaction with β-diketo oxygens, stabilizing the synthesized compound; said findings are also in agreement with the optimized geometry shown by DFT calculations and observations from IR spectrum.

Thermal Properties. Thermogravimetric Analysis (TGA) and Differential Scanning Calorimetry (DSC) were performed to investigate the thermal stability, temperature-dependent decomposition, and presence of any coordinated hydration sphere, as predicted by computational calculations. TGA thermogram of α-Mercurin (Supporting Information Figure S13) showed initiation of pyrolytic degradation ∼ 100 °C that ended at 800 °C. TGA thermogram also exhibited reduced thermal stability and increased amorphous nature of α-Mercurin, compared to curcumin; similar findings are also observed in powder X-ray diffraction (XRD) data. While the TGA thermogram of hydrophobic curcumin showed no loss of water molecule, α-Mercurin exhibited weight loss finished around 100 °C which is in agreement with a broad endothermic peak having maxima (T_{peak}) at ∼66 °C in the DSC thermogram, which could be attributed to coordinated water molecules[64] (Figure 5a). Another weak endothermic T_{peak} at ∼133 °C with T_{onset} of ∼124 °C could be assigned to dissociation of mercury atom from the compound. DSC thermogram also revealed a strong exothermic T_{peak} at ∼191 °C, which revealed the predominant amorphous nature of α-Mercurin, compared to curcumin; findings are also consistent with powder-XRD analysis. The characteristic XRD peaks of α-Mercurin appearing at diffraction angles (2θ) 5.19°, 10.32°, 15.5°, and 19.9° suggested that none of the characteristic Bragg peaks of curcumin are present in the diffractogram of α-Mercurin (Figure 5b), indicating formation of amorphous structure due to bonding of mercury.

Electronic Structure. Furthermore, X-ray photoelectron spectroscopy (XPS) was performed to evaluate the electronic structure of the synthesized compound, compared to that of curcumin[65,66] (Figure 5c). The XPS measurements were carried out for the core-level electrons of carbon, oxygen, and mercury atoms. Photoemission from 1s core level carbon (C 1s) environments of curcumin resulted in four components for sp^2 carbon, sp^3 carbon, C−O, and C═O at 284.12, 286.96, 288.81, and 290.67 eV, respectively (Figure 5d). However, the deconvolution of carbon (C 1s) spectrum of α-Mercurin demonstrated five components with significant changes in the spectral pattern (Figure 5g). A new peak is deconvoluted at 282.59 eV that could be assigned to C−Hg photoemission, mercury being the newly included and least electronegative bonding partner of carbon in the synthesized structure. Further, photoemission signals for C−C, C−O, and C═O are shifted to higher binding energy (B_E), from 286.96, 288.81, and 290.67 eV in curcumin to 288.91, 290.05, and 291.71 eV, respectively, in α-Mercurin. These higher energy shifts are due to the metalation of α-carbon, affecting electron density on adjacent carbon atoms in the compound, which is consistent with deshielding observation from the NMR study.

The XPS photoemission of oxygen (O 1s) for curcumin is distributed from 527 to 540 eV and deconvoluted into two components, with peaks at 531.5 and 534.96 eV, those could be assigned to C−O and C═O environments, respectively (Figure 5e), while the B_E distribution of oxygen (O 1s) for α-Mercurin is having broader distribution, over the range of 525−541 eV and deconvoluted into two components, with peaks at 531.5 and 536.85 eV (Figure 5h). Therefore, binding energy for C−O, assigned to the peak at 531.5 eV remains unchanged in O 1s spectra, while the peak in higher B_E at 534.96 eV further shifted to 536.85 eV due to interaction with mercury (C═O···Hg). This upfield shift indicates loss of electronic screening of oxygen nucleus, as suggested by DFT and NMR studies. The electron density increase around α-carbon caused electron cloud pull from β-carbons, resulting in a deshielded environment; further, β-carbons in turn attract the electron cloud from the oxygen atoms, leading to the loss of electronic screening of oxygen nucleus. Furthermore, the loss of screening increases due to distal coordination between oxygen and mercury (O···Hg). The above-mentioned effects in combination resulted to a higher binding energy shift for C═O.

Photoemissions from 4f and 4d levels of mercury environments of α-Mercurin resulted in two pairs of chemically shifted peak components, each having spin−orbital splitting, confirming the involvement of two atomic partners. Following previous literature, components with B_E of 99.8 and 103.69 eV with ΔeV of ∼4 could be assigned to $4f_{7/2}$ and $4f_{5/2}$ photoemission from Hg···O environment[67,68] (Figure 5f). Similarly, from 4d level, the components at 359.6 and 378.47 eV could also be assigned to Hg···O $4d_{5/2}$ and $4d_{3/2}$ environments (Figure 5i). For 4f level, another pair of components was observed having maxima at 105.94 and 109.84 eV, those could be assigned to C−Hg photoemission; correspondingly, for 4d level, a pair of components was found with peaks at 364.73 and 383.89 eV, supporting the interaction between C and Hg orbitals. From the C 1s photoemission, we already analyzed the presence of a new component at 282.83 eV, assigned to C−Hg environment. The α-carbon, being bonded to mercury, could polarize the valence shell electron cloud toward itself, resulting in the loss of electronic shielding around mercury nucleus, which is also consistent with the charge distribution from DFT calculation as well as the NMR study. Thus, XPS analysis in combination with NMR study and DFT calculations confirmed the bonding of mercury and α-carbon via coordinate covalent bonding, along with distal coordination between mercury and keto oxygens, providing stability to the synthesized compound.

Anticancer Properties, In Vitro. The cytotoxicity of α-Mercurin was evaluated on human acute lymphoblastic leukemia (ALL) cells MOLT-4 and human acute promyelocytic leukemia (AML) cells HL-60, comparing to healthy human PBMCs (Supporting Information Figure S22) by cell viability assay, using MTT (3-(4,5-dimethyl-2-thiazolyl)-2,5-diphenyl-2-H-tetrazolium bromide) reagent, in vitro. Results

https://doi.org/10.1021/acsomega.4c10710
ACS Omega 2025, 10, 17416−17434

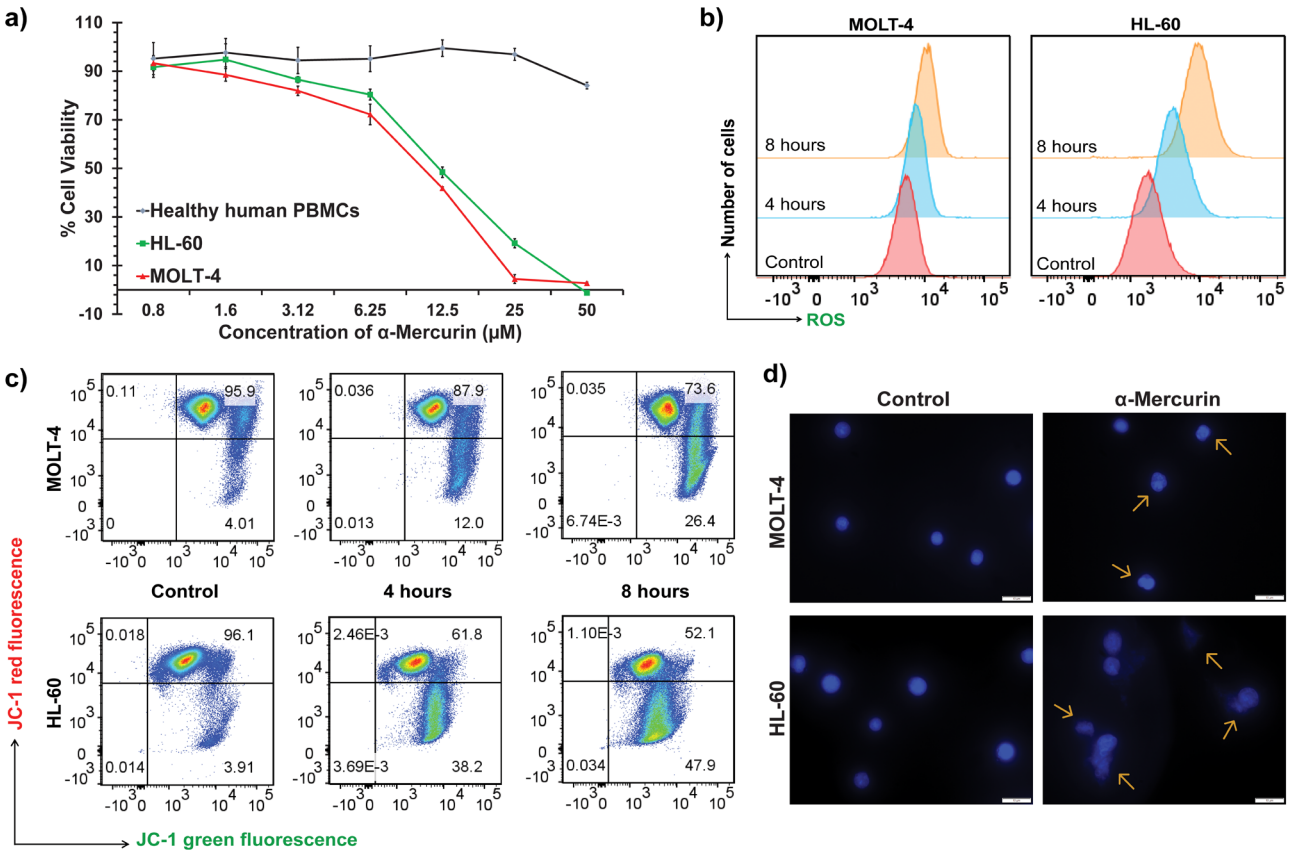

Figure 6. (a) Cytotoxicity of α-Mercurin was investigated on MOLT-4, HL-60 and healthy human PBMCs, using MTT assay. α-Mercurin shows selective cytotoxicity against both the acute leukemia cell lines, in vitro, comparing to healthy human PBMCs, ex vivo. (b) Representative data of MOLT-4 and HL-60 cells showing changes in DCF fluorescence intensity, in vitro. DCF fluorescence intensity increases in a time dependent manner after α-Mercurin treatment for 4 and 8 h, indicating an increase in the intracellular ROS level. (c) Flow cytogram of MMP assay on MOLT-4, and HL-60 cells after 4 and 8 h of α-Mercurin treatment, in vitro. Green fluorescence intensity of JC-$1_{monomer}$ increases while red fluorescence of JC-$1_{aggregate}$ decreases in a time dependent manner, suggesting depolarization of MMP. (d) Fluorescence microscopic images of MOLT-4 and HL-60 cells after 16 h of treatment with α-Mercurin, in vitro, followed by DAPI staining; yellow arrows showing nuclear compaction and fragmentation. Scale bar: 10 μm.

demonstrated (Figure 6a) dose-dependent cytotoxicity of α-Mercurin, selectively on MOLT-4 and HL-60 cell lines without significant cytotoxicity on human healthy PBMCs. Low dose toxicity was observed on both MOLT-4 and HL-60 cells after 96 h treatment, half-maximum inhibitory concentration (IC_{50}) = 10.76 ± 0.23 and 12.48 ± 0.55 μM, respectively. Cell viability using Calcein-AM staining with fluorescence microscopy (Supporting Information Figure S23) also showed that α-Mercurin can eliminate acute leukemia cells in a dose-dependent manner.

The potential effect of α-Mercurin on the intracellular ROS level was investigated using flow cytometry. MOLT-4 and HL-60 cells were treated with 20 μM α-Mercurin, and oxidative stress was measured by staining with 2′,7′-dichlorodihydrofluorescein diacetate (DCFH-DA). Corresponding results suggested that the synthesized compound can increase intracellular ROS levels in a time-dependent manner (Figure 6b). For both MOLT-4 and HL-60 cells, there is a significant increase in the green fluorescence intensity in the presence of α-Mercurin, compared to no treatment, after 8 h.

To investigate the effect of α-Mercurin on mitochondrial transmembrane potential (MMP), lipophilic cationic dye 5,5′,6,6’ -tetrachloro-1,1′,3,3′-tetraethylbenzimi-dazoylcarbocyanine iodide (JC-1) was used to measure depolarization of MMP in both MOLT-4 and HL-60 cells via flow cytometry. After treatment with 20 μM compound for 4 and 8 h, cells were further incubated with 20 μM JC-1 for 30 min. As the MMP depolarized with time, green fluorescence of JC-1 monomer increased, while red fluorescence from JC-1 aggregate decreased. Flow cytometric results (Figure 6c), including JC-1 red/green fluorescence ratio (Supporting Information Figure S25), demonstrated that α-Mercurin can induce apoptosis in acute leukemia cells, by decreasing MMP, via intrinsic pathway.

To study the nuclear compaction and fragmentation after treatment with α-Mercurin, 4′,6-diamidino-2-phenylindole (DAPI) staining was performed. After treatment with 20 μM of the compound for 16 h, MOLT-4 and HL-60 cells were stained with 300 nM DAPI and incubated in dark. Fluorescence microscopic images (Figure 6d) suggested that nuclear morphologies of control cells are well-defined and intact, while treated cells exhibited significantly fragmented and condensed nuclei.

The effect of α-Mercurin on cell cycle progression was investigated by flow cytometry with propidium iodide (PI) staining. MOLT-4 and HL-60 cells were treated with 20 μM compound for 4, 8, and 16 h. Cells were then harvested and fixed with 70% ice-cold ethanol prior to PI staining. Compared to untreated cells, α-Mercurin causes a remarkable increase in the S phase population (MOLT-4 = ∼26 to ∼44% and HL-60

https://doi.org/10.1021/acsomega.4c10710
ACS Omega 2025, 10, 17416−17434

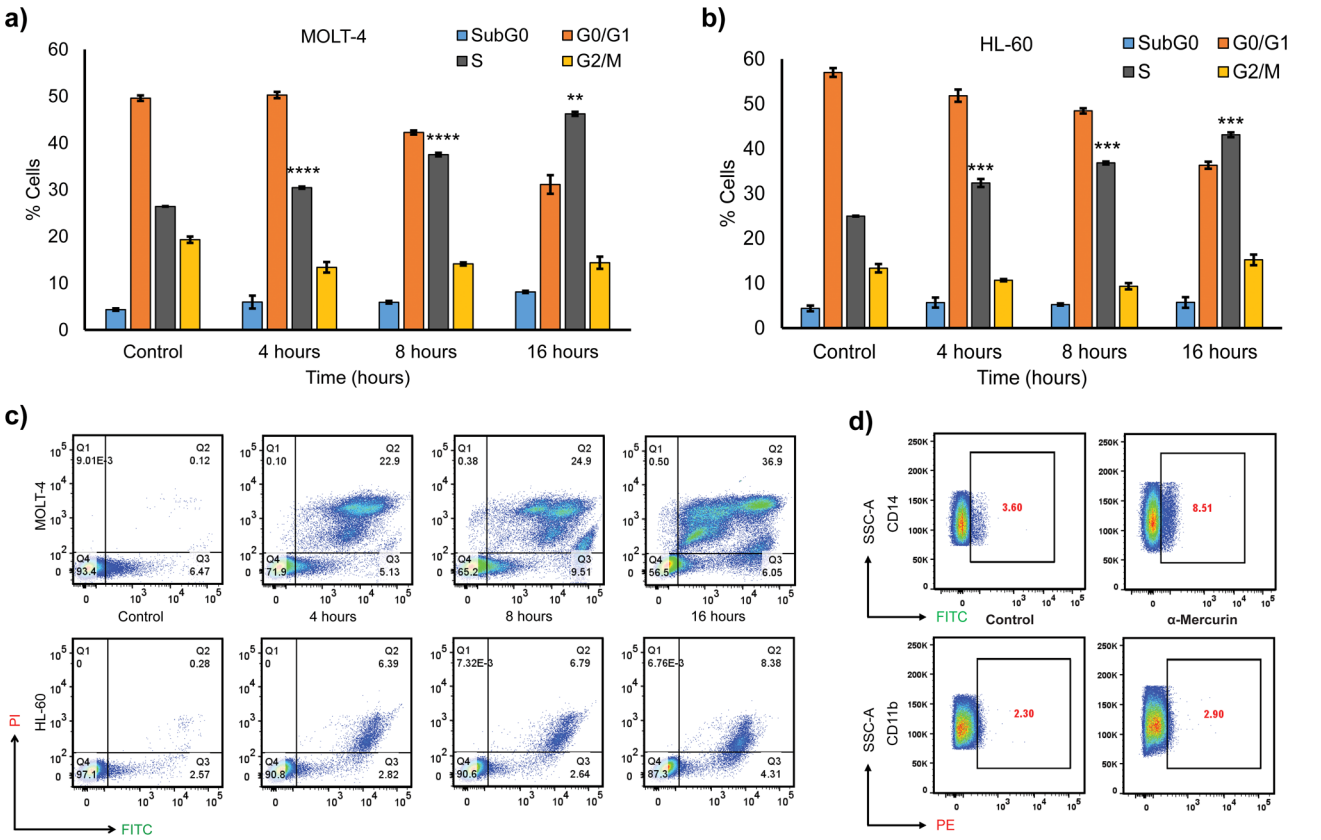

Figure 7. (a,b) Cell cycle analysis of MOLT-4 and HL-60 cells after α-Mercurin treatment for 4, 8, and 16 h. Cells were fixed and stained with PI prior flow cytometric ananlysis. Percent of cell population in different phases of cell cycle were recorded. The analysis was repeated 3 times and results are represented as mean ± SEM (n = 3, *P < 0.05; **P < 0.01; ***P < 0.001; Student's t test). (c) Apoptosis/necrosis assay of α-Mercurin on MOLT-4 and HL-60 cells after 4, 8, and 16 h of treatment, in vitro. Flow cytometric analysis suggests an increase in both early and late apoptotic populations for both cell lines. Cells were stained with FITC-Annexin-V and PI. The Q4 quadrant (Annexin V−/PI−), Q3 quadrant (Annexin V+/PI−), Q2 quadrant (Annexin V+/PI+), and Q1 quadrant (Annexin V−/PI+) indicate the percent of normal healthy cells, early apoptotic, late apoptotic, and necrotic cells, respectively. (d) Representative flow cytogram of changes in expression pattern of differentiation marker CD14 and CD11b on healthy human granulocytes after treatment with α-Mercurin for ∼16 h; suggesting significant increase in CD14 expression.

= ∼25 to ∼42%), including corresponding reduction in the G_0/G_1 population (MOLT-4 = ∼49 to ∼31% and HL-60 = 57 to ∼36%). Therefore, α-Mercurin can arrest cell cycle at the S phase in a time-dependent manner (Figure 7a, b).

The mode of cell death upon α-Mercurin treatment was further investigated on both MOLT-4 and HL-60 cells by flow cytometry. Time-course analysis (4, 8, and 16 h) of cells treated with α-Mercurin followed by fluorescein isothiocyanate-annexin-V/propidium iodide (FITC-AV/PI) staining suggested increase of cell population in early as well as late apoptosis. However, no necrotic population was found, confirming that the compound induced cell death via apoptotic pathway. In case of MOLT-4 cells, as time progressed, apoptotic population with different morphology appeared in late and early apoptotic populations, as observed in Q2 and Q3, respectively. For HL-60 cells, single apoptotic population was observed, both in late and early apoptosis across Q2 and Q3 (Figure 7c).

The expression of cell differentiation markers CD14 and CD11b was investigated on MOLT-4, HL-60 as well as healthy human blood cells, excluding RBC. Cells were treated with 20 μM α-Mercurin for ∼16 h and further stained with FITC-CD14 and PE-CD11b antibodies, prior to flow cytometric analysis. Results demonstrated no significant changes in differentiation marker expression for both MOLT-4 and HL-60 cells, upon α-Mercurin treatment (Supporting Information Figures S26 and S27). Interestingly, the compound treatment showed a significant increase of CD14 expression in the granulocyte population (Figure 7d), while no change in CD11b expression. Results also showed no notable change in CD14 as well as CD11b expression for the lymphocyte population (Supporting Information Figure S28). Therefore, α-Mercurin can induce the expression of differentiation marker for WBCs.

The above results demonstrated that treatment with α-Mercurin increased intracellular ROS levels, which may reduce mitochondrial transmembrane potential and arrest the cell cycle at the "S" phase. All of these damages collectively induced apoptosis in acute leukemia cells, as observed from nuclear fragmentation and apoptosis assay. Changes in the expression patterns of cell differentiation markers also suggested the potential of α-Mercurin for immunomodulation.

Potential of the Compound, Ex Vivo. To assess the antileukemia potential of α-Mercurin in a clinically relevant context, we investigated the effect of the compound on PBMCs isolated from ALL patients' blood samples (n = 11). Samples were collected from patients of all ages and sexes before initiation of any clinical treatment. PBMCs were maintained in

https://doi.org/10.1021/acsomega.4c10710
ACS Omega 2025, 10, 17416−17434

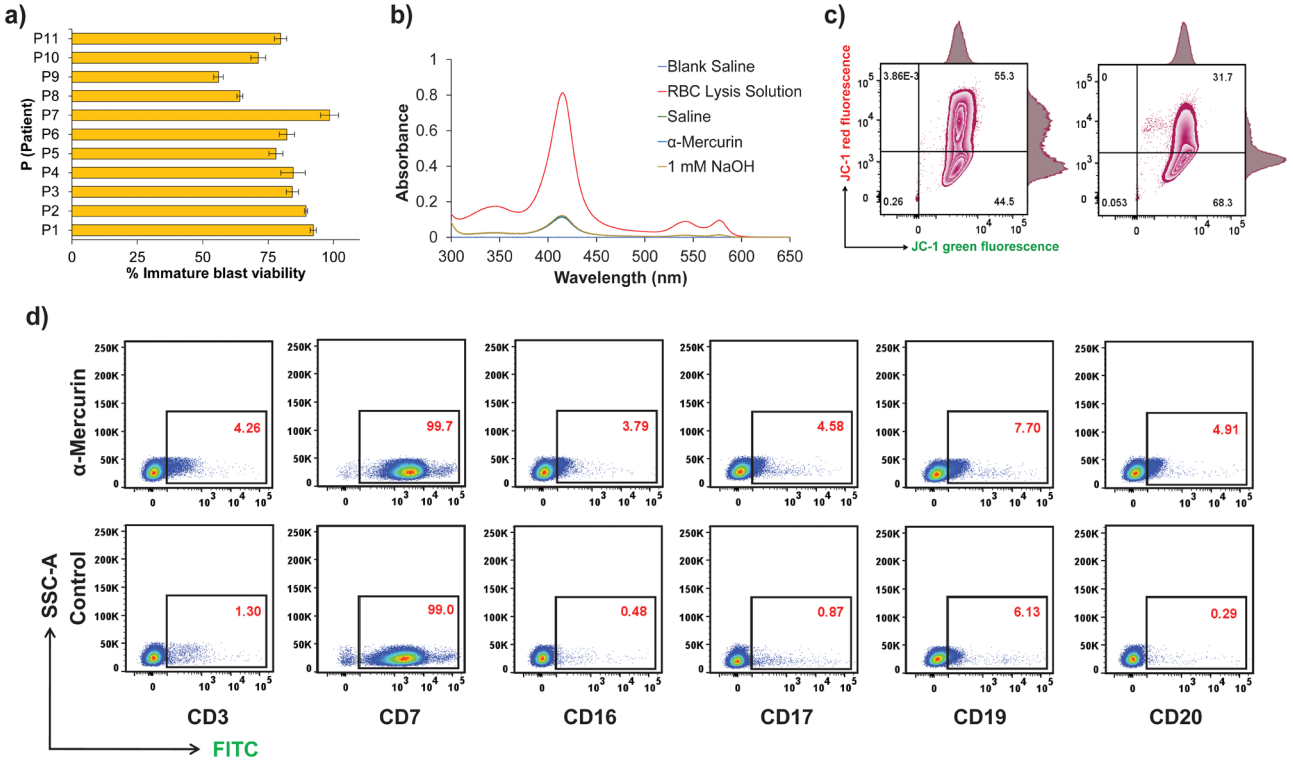

Figure 8. (a) Cytotoxic potential of α-Mercurin on immature leukemic blasts, isolated from ALL patients' blood samples. Viability data suggests that α-Mercurin treatment for 72 h can eliminate ~20 ± 4% immature leukemic blasts, without causing significant toxicity to healthy lymphocytes, ex vivo (n = 11, individual experiments). (b) Representative UV−visible spectroscopic data of erythrocyte hemolysis assay suggests no significant hemolysis caused by α-Mercurin treatment compared to RBC lysis solution, ex vivo. (c) Representative flow cytogram of MMP assay on immature blasts from ALL patients, ex vivo, upon α-Mercurin treatment for 72 h. Experimental results suggest, significant depolarization of MMP. (d) Representative flow cytogram of expression pattern for different CD markers present on B and T lymphocytes of ALL patients PBMCs, after treatment with α-Mercurin, ex vivo. The immunogenic expression after treatment were compared to control groups, suggesting increased expression patterns of CD markers, upon α-Mercurin treatment.

RPMI-1640 medium, containing 10% FBS, and treated with 20 μM compound for 72 h; cell viability analysis was performed, using flow cytometry. α-Mercurin demonstrated notable cytotoxic activity and eliminated ~ 20 ± 4% of immature leukemic blasts, without causing significant toxicity to healthy lymphocytes, ex vivo (Figure 8a). The cytotoxic potential of α-Mercurin observed, ex vivo, is in agreement with the findings from the in vitro study on acute leukemia cells. Erythrocyte hemolysis assay was performed on whole blood samples to investigate potential toxicity on RBCs. The whole blood collected from leukemia patients was treated with RBC lysis buffer, saline, 20 μM α-Mercurin, and 1 mM NaOH, followed by incubation for 20 min at 37 °C, then centrifuged; UV−visible spectra of the supernatants were collected for the region, 300−650 nm. Results suggested no significant hemolysis for α-Mercurin treatment (Figure 8b), in any case (n = 11), compared to the RBC lysis solution (positive control).

Depolarization of MMP of immature blasts from leukemia patients due to α-Mercurin treatment, ex vivo, was analyzed using flow cytometry with JC-1 staining. PBMCs isolated from ALL patients were treated with 20 μM α-Mercurin and incubated for 72 h. Cells were further harvested and incubated with 20 μM JC-1 dye for 30 min, followed by flow cytometric analysis. The data set suggested that mitochondrial transmembrane potential for the leukemic blast populations from ALL patients got significantly depolarized upon the compound treatment (Figure 8c), and may induce apoptosis via intrinsic pathway.

The role of α-Mercurin on immunomodulation was also analyzed by treating ALL patients' PBMCs, ex vivo. PBMCs were treated with 20 μM synthesized compound and incubated for 72 h. Expression patterns of the following CD markers, CD16, CD17, CD3, CD7, CD19, and CD20 were analyzed by flow cytometry. During clinical diagnosis, expression patterns of different immunogenic markers considered in the study were heterogeneous among different patients, depending on stages of the disease and other hematological parameters. Overall expression patterns (Supporting Information Table S9) of CD markers (CD3, CD7, CD19, and CD20) having crucial role in immunogenic response increased, upon α-Mercurin treatment, as demonstrated in the representative flow cytometric analysis (Figure 8d). Said immunogenic markers are especially involved in B as well as T cell development and activation; CD19 and CD20 for B cells and CD3 for T cells.

Subacute Toxicity, In Vivo. Subacute toxicity of α-Mercurin was routinely investigated on Swiss albino mice. α-Mercurin was administered intravenously into the lateral tail vein of 4 Swiss albino mice, twice a week for 8 weeks (Figure 9a), while the control group was injected with sterile saline. 80 μL of 2 mM α-Mercurin (~3.3 mg/kg body weight) was injected into each mouse at each session throughout the study. All injections were smooth with steady fluid movement and no allergic reaction or anaphylactic shock was observed. Following injection, each mouse was closely monitored for their behavior,

https://doi.org/10.1021/acsomega.4c10710
ACS Omega 2025, 10, 17416−17434

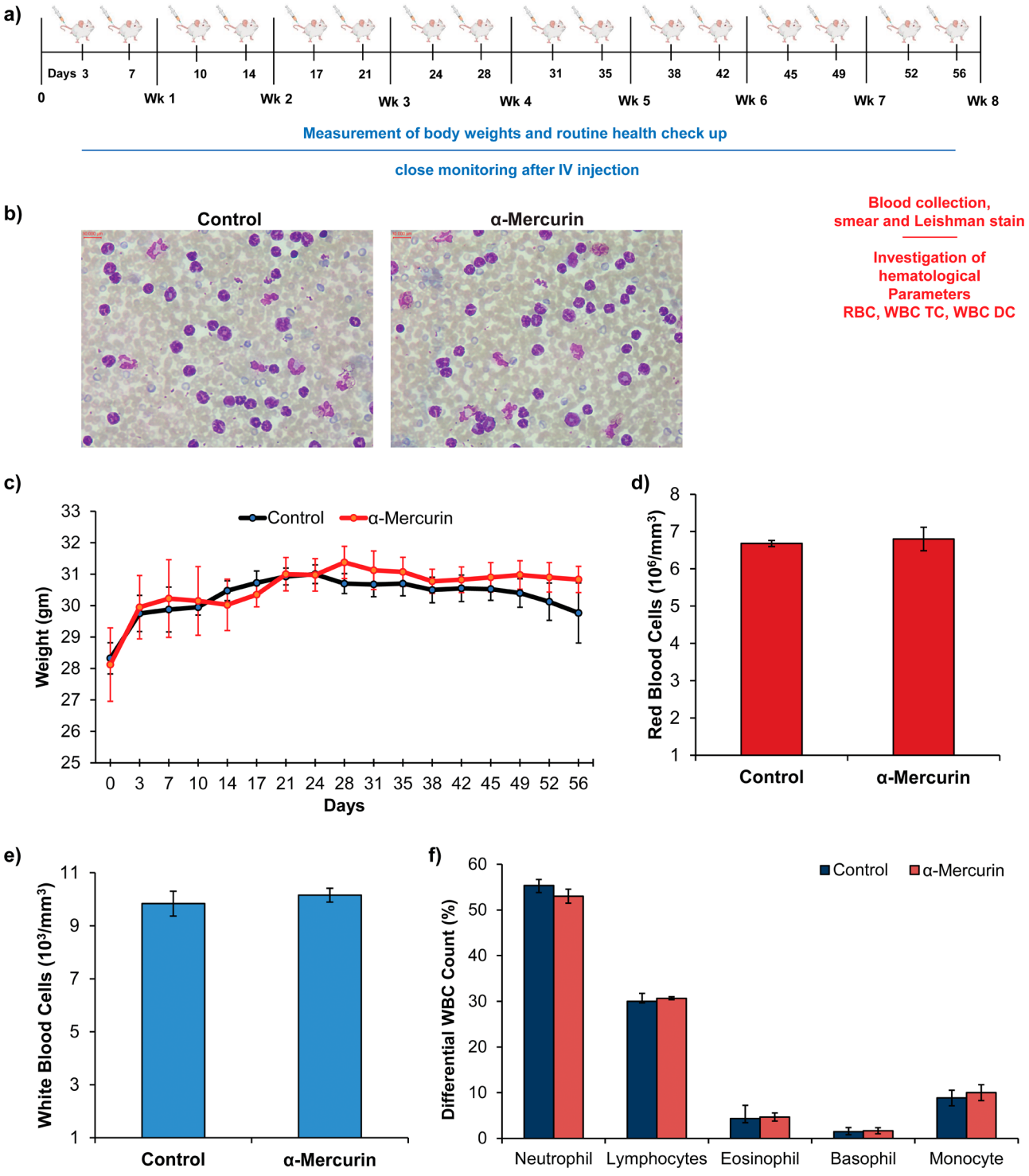

Figure 9. (a) Investigation of subacute toxicity of α-Mercurin on swiss-albino mice. 80 μL of the compound solution was intravenously injected from a 2 mM stock; twice a week for 8 weeks. All animals were observed regularly for general health and symptoms of any toxicity, whereas body weight changes were recorded on days of injection; 0, 3, 7, 10, 14, 17, 21, 24, 28, 31, 35, 38, 42, 45, 49, 52, and 56 of the experiment. At the end of the study, all animals were kept in fasting, overnight before blood sampling for examination of hematological parameters. (b) Representative stained (Leishman's stain) blood smear of control and α-Mercurin treated animals after 8 weeks of treatment. (c) Graphical representation of body weight analysis during toxicity study demonstrating no weight loss as well as no statistical difference between body weights of treated and control groups. (d) Comparative analysis of RBC count from blood samples of α-Mercurin treated and control group animals, suggesting no toxicity on erythrocytes. (e) Comparative analysis of total WBC count, suggesting total WBC count is remaining within the normal range after treatment. (f) Differential leukogram suggesting no significant difference between treatment and control groups.

agility, breathing, and pain/discomfort. No notable behavioral change, compared to the control group was observed (Supporting Information Figure S31, Videos S1 and S2). Additionally, no significant changes in food and water consumption were observed. Representative Leishman's stained blood smear of control and α-Mercurin treated animals

https://doi.org/10.1021/acsomega.4c10710
ACS Omega 2025, 10, 17416−17434

also suggested no significant difference in appearance, number, and morphology of blood cells (Figure 9b). Body weight evaluation suggested no notable weight loss in any group during the study and no significant difference between the treated and control group, with an average body weight of ∼30.5 g (Figure 9c). No gross physiological changes were observed in the kidney, liver, stomach, lungs, spleen, heart, thymus, and lymph nodes in the experimental group, compared to the control group (Supporting Information Figure S32). The analysis of hematological parameters, including total RBC (Figure 9d), total WBC (Figure 9e), and differential WBC (Figure 9f) count showed similar patterns between the treated and control groups, with no statistically significant difference. In summary, a toxicity study with repeated dosing, in vivo, suggested no subacute toxicity, including normal behavioral patterns, body weight, and hematological parameters.

CONCLUSIONS

We developed a novel organometallic compound by bonding mercury to the α-carbon of curcumin, along with distal coordination involving keto oxygen for the treatment of acute leukemia, and named it α-Mercurin. It is the first organometallic compound of curcumin where a metal atom is directly bonded to α-carbon providing protection at alkaline pH in aqueous medium and could be dissociated at acidic environment, in the presence of amphipathic molecules. α-Mercurin demonstrated selective cytotoxicity against ALL and AML cells, in vitro, as well as immature blasts from ALL patients, ex vivo, without causing significant toxicity toward healthy PBMCs. Further, α-Mercurin showed no hemolytic effect on human blood samples and also demonstrated potential for inducing granulocyte differentiation. In terms of mechanism of action, flow cytometric analysis suggested that it can increase intracellular ROS levels, and eliminate both ALL and AML cells via intrinsic pathway of apoptosis, in vitro. α-Mercurin can also reduce mitochondrial transmembrane potential, in vitro as well as ex vivo. Furthermore, repeated intravenous administration of α-Mercurin showed no subacute toxicity, including body weight, behavioral pattern, and hematological parameters. To the best of our knowledge, it is the first organometallic compound of curcumin as well as mercury that is suitable for intravenous administration in the molecular form, without anaphylactic shock and subacute toxicity. In the next phase of our work, we will investigate the comprehensive efficacy of α-Mercurin, including biodistribution and immunomodulatory properties on rat model, induced for acute leukemia.

In ancient Ayurveda and traditional Chinese medicine, the divalent metal ion mercury was profoundly used to treat hematological disorders, but its application in modern medicine is restricted due to systemic toxicities.[69−73] In this study, we delivered mercury in an organometallic formulation and demonstrated no toxic effect on healthy blood cells. The innovative bonding strategy of our work should allow researchers to investigate other metal atoms in conjunction with curcumin to form aqueous soluble structures with sufficient stability. Therefore, we believe that the present study will pave a way for designing mercury as well as curcumin-based therapeutics for the treatment of acute leukemia and other malignancies. Furthermore, α-Mercurin also showed its potential as an immunomodulator and could be explored for immunotherapy, in combination with other chemotherapeutics.

EXPERIMENTAL SECTION

Instruments Used. Type-I water was used from a Simplicity Water Purification System (Merck-Millipore). All other solvents and reagents were purchased commercially and used without further purification unless specified. Solvents were degassed when needed, using a water bath sonicator. All antibodies were used at concentrations instructed by the manufacturer. All UV−visible spectra were recorded on a Thermo Evolution 350 spectrophotometer. Fluorescence emission spectra were recorded on a Cary Eclipse fluorescence spectrophotometer at room temperature. HPLC separation was performed in a NOVA PAK C_{18} column by isocratic elution with water and acetonitrile (v/v, 35:65) using a Waters-1525 Binary HPLC Pump. The elution was monitored by observing the absorbance at 426 nm with a Waters-2489 UV/Visible Detector. High-resolution mass spectrum (HRMS) was recorded by an LTQ Orbitrap XL mass spectrometer (Thermo Scientific). Electrospray Ionization Mass Spectrum (ESI−MS) was recorded by a Xevo G2-XS QTof mass spectrometer (Waters). IR spectra were recorded on a Bruker Tensor 27 FT-IR ATR, using a thin film of a dry sample. Thermogram of thermogravimetric analysis (TGA) was recorded with a TGA 400 (PerkinElmer) Analyzer. Differential Scanning Calorimetry (DSC) was done using a DSC 8000 (PerkinElmer) instrument with heating rate of 10 °C/min. ^{1}H, ^{13}C, ^{13}C-DEPT, 2D ^{1}H−^{1}H NOESY, 2D ^{13}C−^{1}H HMBC and 2D ^{13}C−^{1}H HSQC NMR spectra in DMSO-d_6 and D_2O (10 mM NaOH) were recorded on Bruker Avance (III) 600 MHz and Jeol Resonance 400 MHz NMR spectrometers at room temperature (∼298 K). All chemical shifts are given relative to tetramethyl-silane (TMS). Solid state ^{13}C CP/MAS and ^{1}H NMR spectra were recorded on a Jeol 500 MHz NMR spectrometer equipped with a 4 mm HXMAS4 Probe at room temperature (∼298 K). Chemical shifts (δ) are given in parts per million (ppm), and coupling constants (J) are given in hertz (Hz). XPS spectra were recorded using a ULVAC PHI 5000 VERSA PROBE III equipped with a monochromatic Al X-ray source and focused beam. Powder XRD data were recorded using a BRUKER D8-Advance. All centrifugations during the synthesis of the compound were done using a REMI NEYA 16R centrifuge and centrifugations during PBMC isolation were done in a HERMLE cold centrifuge at 18 °C. The absorbance for the MTT assay was measured using a TECAN Infinite M200 PRO ELISA plate reader at 570 nm. Cell viability with Calcein-AM staining and nuclear fragmentation with DAPI staining were investigated using an Olympus BX53 Digital Upright Microscope. All flow cytometry were performed on a BD LSRFortessa flow cytometer.

Reagents and Chemicals. Curcumin (Sigma-Aldrich, Cat No. C7727), mercury(II) chloride (Sigma-Aldrich, Cat No. 215465), ammonium hydroxide (Supelco, Cat No. 1935000521), iron(III) chloride anhydrous (Supelco, Cat No. 1936530521), L-glutathione reduced (Sigma-Aldrich, Cat No. G4251-1G), CD_3OD/methanol-d_4 (Sigma-Aldrich, Cat No. 151947), D_2O/deuterium oxide (Merck, Cat No. 151882), deuterated dimethy sulfoxide/DMSO-d_6 (Sigma-Aldrich, Cat No. 151874), Roswell Park Memorial Institute (RPMI) 1640 medium (Gibco BRL, Cat No. A10491-01), fetal bovine serum (FBS, Gibco BRL, Cat No. 10082-147, 10% v/v), penicillin-streptomycin-glutamine (Gibco BRL, Cat No. 10378-016, 1% v/v), gentamicin (Abbott, 50 μg/mL), 3-(4,5-dimethyl-2-thiazolyl)-2,5-diphenyl-2-H-tetrazolium bromide

https://doi.org/10.1021/acsomega.4c10710
ACS Omega 2025, 10, 17416−17434

(MTT) (Sigma-Aldrich, Cat No. M2128), dimethyl sulfoxide (DMSO, Supelco; Cat No. 1.167430521), calcein-AM (Invitrogen, Cat No. C1430, final conc. 1 μM), 2′,7′-dichlorodihydrofluorescein diacetate (DCFH-DA, Abcam; Cat No. ab113851, final conc. 5 μM), 5,5′,6,6′-tetrachloro-1,1′,3,3′-tetraethylbenzimi-dazoylcarbocyanine iodide (JC-1, Sigma, Cat No. T4069G, final conc. 20 μM), 4′,6-diamidino-2-phenylindole (DAPI, Invitrogen, Cat No. D1306, final conc. 300 nM), Annexin-V apoptosis kit (Invitrogen, Cat No. A13199, 2 μL of annexin-V, PI solution conc. 50 μg/mL), RNase A Solution (HIMEDIA, Cat No. DS0003, final conc. 100 μg/mL), K2-EDTA (K2E) 10.8 mg blood collection tubes (BD Vacutainer; Cat No. 367863), Ficoll-Paque PLUS solution (Cytiva; Cat No. 17144002). Primary antibodies; FITC mouse anti-human CD14 (BD, Cat No. 347493), PE mouse anti-human CD11b (BD, Cat No. 347557), CD16 (Abcam; Cat No. ab183354), CD17 (Invitrogen; Cat No. MA1- 10118), CD3 (Abcam; Cat No. ab186669), CD7 (Abcam; Cat No. ab224194), CD19 (Abcam; Cat No. ab254170), CD20 (Abcam; Cat No. ab9475). Secondary antibodies; goat anti-rabbit IgG H&L (Alexa Fluor 488) preadsorbed (Abcam; Cat No. ab150081), goat anti-rabbit IgM mu chain (Alexa Fluor 488) (Abcam; Cat No. ab150093), and goat anti-mouse IgG H&L (Alexa Fluor 488) preadsorbed (Abcam; Cat No. ab150117).

Synthesis. 1,7-Bis(4-hydroxy-3-methoxyphenyl) hepta-1,6-diene-3,5-dione (Curcumin) was dissolved in 95% ethanol (C_2H_5OH:H_2O = 95:5) at final concentration of 1 mM and kept overnight in stirring condition. Next morning, the solution was taken in a borosilicate round-bottom flask and placed over a magnetic stirrer at room temperature (~25 °C); then, ammonium hydroxide (NH_4OH) was added dropwise until the pH of the solution reached 8.2−8.4 and incubated for 10 min in dark. Then, aqueous solution of 184 mM mercury(II) chloride (50 mg/mL) was added at a molar ratio of curcumin: $HgCl_2$ = 1:8. The mixture was then incubated on a magnetic stirrer for 4 h at room temperature (~25 °C). After 4 h of incubation, the reaction mixture was centrifuged and the pellet was further washed five times with ethanol and once with Type-I water. The pellet was then dried at room temperature (~25 °C) or using a lyophilizer and resuspended in DMSO or aqueous 10 mM NaOH solution, depending upon experimental requirements. Yield = 95%. ^{1}H NMR (600 MHz, DMSO-d_6, 20 mg, 50 mmol) δ = 9.61 (s, 2H), 7.35 (d, J = 15.5 Hz, 2H), 7.26 (s, 2H), 7.23 (d, J = 6.2 Hz, 2H), 7.11 (d, J = 6.2 Hz, 2H), 6.81 (d, J = 8.1 Hz, 2H), 3.81 (s, 6H). ^{13}C NMR (151 MHz, DMSO-d_6, 20 mg, 50 mmol): δ = 194.73, 149.01, 147.90, 139.27, 126.49, 124.59, 122.85, 115.79, 111.62, 96.39, 55.77. Elemental analysis calculated for α-Mercurin: C = 44.38, O = 16.89, Hg = 35.3; found: C = 44.6, O = 17.7, Hg = 36.1. HR-MS (anion): m/z calculated = 579.1907 ($C_{21}H_{18}O_6Hg + OH^-$); found = 579.1253. ESI-MS (anion): m/z calculated = 627.1739 ($C_{21}H_{16}O_6Na_2Hg + OH^-$); found = 627.0839.

1,7-Bis(4-hydroxy-3-methoxyphenyl) hepta-1,6-diene-3,5-dione (Curcumin): ^{1}H NMR (600 MHz, DMSO) δ 16.39 (s, 1H), 9.65 (s, 2H), 7.55 (s, 2H), 7.32 (s, 2H), 7.15 (s, 2H), 6.82 (s, 2H), 6.75 (s, 2H), 6.06 (s, 1H), 3.84 (s, 6H). ^{13}C NMR (151 MHz, DMSO) δ: 183.33, 149.44, 148.12, 140.84, 126.46, 123.26, 121.20, 115.82, 111.38, 101.01, 55.81.

Computational Details. All the optimizations and calculations were performed by the Gaussian09[74] program at the level of density functional theory (DFT). The structure was optimized by generalized gradient approximation exchange-correlation density functional B3PW91, the basis set of SDD for Hg atom and 6-31G(d)[75] for other atoms were chosen to describe all the atoms. The solvent effect was included with self-consistent reactions field (SCRF) based on the SMD[76] model, where ethanol, dimethyl sulfoxide, and water were set as the solvent models in order to mimic the experimental conditions. The keyword "pseudo = read" was used for α-Mercurin to include effective core potentials (ECPs or pseudopotentials) for the organometallic system.

Cell Lines and Culture Conditions. The human acute lymphoblastic leukemia cell line (MOLT-4) and the human acute promyelocytic leukemia cell line (HL-60) were obtained from the National Centre for Cell Science (Pune, India). The human peripheral blood mononuclear cells (PBMCs) were isolated from whole blood as per general guidelines. For the isolation of PBMCs, ~4 mL of blood was collected from individuals in K2-EDTA (K2E) 10.8 mg blood collection tubes and diluted with sterile PBS at the ratio of whole blood: PBS = 1:2. Further, Ficoll-Paque PLUS solution was taken in a sterile tube at a volumetric ratio of whole blood: ficoll = 2:3 and the diluted blood was carefully layered upon the solution by avoiding intermingling of two phases. Further, the tube was centrifuged using a swinging bucket rotor for 25 min at 400×g at 18 °C in a HERMLE cold centrifuge. Following centrifugation, the cloudy-looking phase in between ficoll and plasma was collected and further washed with sterile PBS by centrifuging at 100×g for 10 min at 18 °C. For the differentiation marker (CD14 and CD11b) expression analysis, ~4 mL blood samples were collected from healthy individuals in K2-EDTA blood collection tubes. Furthermore, the blood samples were treated with 1X RBC lysis solution at the ratio of whole blood: 1X RBC lysis solution = 1:10 (v/v). Followed by 15 min incubation in dark, tubes were centrifuged at 450×g for 5 min at room temperature. Supernatants were discarded, and cells were washed twice with sterile PBS by centrifuging at 450×g for 5 min at room temperature. All the cells were incubated in Roswell Park Memorial Institute (RPMI) 1640 medium supplemented with 10% Fetal Bovine Serum (FBS), 1% (v/v) Penicillin-Streptomycin-Glutamine and 50 μg/mL Gentamicin, at 37 °C under 5% CO_2 and 95% air in a humidified atmosphere.

Cell Viability Analysis Using MTT Assay, In Vitro. Cell viability and IC_{50} were determined using the MTT (3-(4,5-dimethyl-2-thiazolyl)-2,5-diphenyl-2-H-tetrazolium bromide) reagent. Briefly, MOLT-4 and HL-60 cells (5×10^3 cells/well) were seeded in 96-well plates and treated with α-Mercurin as well as curcumin at different concentrations (50, 25,12.5, 6.25, 3.125, 1.6, and 0.8 μM) for 96 h. The 'no treatment' (NT) groups were treated with only media while the "vehicle control" (VC) groups were treated with 1 mM NaOH solution. MTT reagent dissolved in water was added at the final concentration of 0.5 mg/mL and incubated for 4 h. Following incubation, the plates were centrifuged at 400×g for 15 min at 4 °C, protecting from light. The supernatant was exchanged with DMSO to dissolve the formazan crystals, and the absorbance of the wells was measured at 570 nm by a TECAN Infinite M200 Pro microplate reader. The percent of the viable cells (% cell viability) was calculated considering the 'no treatment' (NT) wells as 100% cell survival. All assays were conducted in triplicate and the mean IC_{50} ± standard deviation was determined using Microsoft Excel software (n = 3, *P < 0.05; **P < 0.01; ***P < 0.001; Student's t-test).

https://doi.org/10.1021/acsomega.4c10710
ACS Omega 2025, 10, 17416−17434

Intracellular ROS Assay, In Vitro. DCFH-DA was used for investigation of intracellular ROS level. Briefly, MOLT-4 and HL-60 cells were seeded in 24-well plates (3×10^5 cells/well) and treated with 20 μM α-Mercurin for 4 and 8 h. The control groups were treated with only media. For the positive control, cells were pretreated with H_2O_2. Following incubation, cells were centrifuged at 400xg for 5 min at room temperature (~25 °C) and cell pellets were resuspended in DCFH-DA solution diluted in sterile PBS at the final concentration of 5 μM and incubated for 30 min in dark. At the end of incubation, cells were centrifuged at 400xg for 5 min at room temperature (~25 °C). The supernatant was discarded and cells were again resuspended in 500 μL of sterile PBS. The data were recorded using flow cytometry (BD FACS LSRFortessa) by exciting the samples at 485 nm and emission at 535 nm. All analysis was performed using FlowJo V10.8.1.

Mitochondrial Transmembrane Potential Assay, In Vitro. 5,5′,6,6′-Tetrachloro-1,1′,3,3′-tetraethylbenzimi-dazoyl-carbocyanine iodide (JC-1) was used to measure depolarization of mitochondrial transmembrane potential (MMP). Briefly, MOLT-4 and HL-60 cells (3×10^5 cells/well) were seeded into 24-well plates and treated with 20 μM α-Mercurin for 4 and 8 h. In case of the positive control group, cells were pretreated with a pseudodecoupler, picric acid. Then, 20 μM JC-1 dye dissolved in DMSO was added to each well and incubated for 20 min at 37 °C under 5% CO_2 and 95% air in a humidified atmosphere. Cells were further centrifuged at 400×g for 5 min at room temperature (~25 °C) and cell pellets were resuspended in cold sterile PBS. Flow cytometric analysis was performed using BD LSRFortessa flow cytometer; JC-1_{red} (λ_{ex} = 543 nm, λ_{em}= 575−610 nm), JC-1_{green} (λ_{ex} = 488 nm, λ_{em} = 515−530 nm). All the analysis was performed using FlowJo V10.8.1.

Nuclear Fragmentation Assay, In Vitro. 4′,6-Diamidino-2-phenylindole (DAPI) staining was performed to investigate the nuclear morphology. MOLT-4 and HL-60 cells (3×10^5 cells/well) were seeded into 6-well plates and treated with 20 μM α-Mercurin for 16 h. The control groups were treated with only media. Then, cells were harvested by centrifugation at 400×g for 5 min at room temperature (~25 °C) and further washed with cold sterile PBS. Cells were then resuspended in 300 nM DAPI and incubated for 7 min at room temperature (~25 °C) in dark. Cells were again washed with sterile PBS prior to visualizing under Olympus BX53 Digital Upright Microscope using a fluorescent filter for DAPI, with a 100× objective.

Cell Cycle Analysis, In Vitro. PI staining was used to identify the proportion of cells in different stages of the cell cycle. Briefly, MOLT-4 and HL-60 cells (3×10^5 cells/well) were seeded in 24-well plates and treated with 20 μM α-Mercurin for 4, 8, and 16 h, separately. The control groups were treated with only media. Cells were then collected and fixed using 70% ice-cold ethanol at −20 °C for 20 min. Following fixation, cells were then centrifuged at 400×g for 5 min at room temperature (~25 °C). The supernatants were discarded carefully and 50 μL RNase was added and incubated for 10 min in dark. Next, 350 μL of PI dissolved in sterile PBS was added to the cell suspension and incubated in dark for 5 min before flow cytometric analysis. The data were recorded by a flow cytometer (BD FACS LSR Fortessa). Samples were then excited at 488 nm, and the emission was measured at 575 nm. The assay was repeated three times, and the analysis was performed using FlowJo V10.8.1. Data are exhibited as mean ± SEM (n = 3, *, $P < 0.05$; **, $P < 0.01$; ***, $P < 0.001$; Student's t test).

Apoptosis/Necrosis Assay, In Vitro. MOLT-4 and HL-60 cells (3×10^5 cells/well) were seeded in 24-well plates and treated with 20 μM α-Mercurin for 4, 8, and 16 h, separately. The control groups were treated with only media. The cells were then centrifuged at 400×g for 5 min at room temperature (~25 °C) and supernatants were discarded. Cell pellets were resuspended in cold sterile PBS for washing and centrifuged again under the same condition. The supernatant was discarded and the cell pellets were resuspended in 1× Annexin-V binding buffer provided with the kit, at cell density of 6×10^5 cells/100 μL. Two microliter Annexin-V solution and 1 μL PI solution (100 μg/mL) were added to 100 μL cellular suspension and incubated at room temperature (~25 °C) for 15 min in dark. Further, the 100 μL cellular suspension was diluted to 500 μL using Annexin-V binding buffer. The data were recorded using BD LSRFortessa flow cytometer by exciting the samples at 488 nm and the emission was measured at 530 nm for Annexin-V (FL1) and 575 nm for PI (FL2). All the analysis was performed using FlowJo V10.8.1.

Cell Differentiation Marker Analysis. MOLT-4, HL-60, and healthy human blood cells, excluding RBC were seeded in 6-well plates (3×10^5 cells/well) and treated with 20 μM α-Mercurin for ~16 h. Thereafter, cells were washed twice with sterile PBS by centrifuging at 650×g for 5 min at room temperature (~25 °C). Then, cells were stained with fluorophore-tagged primary antibodies (FITC-CD14 and PE-CD11b) and incubated for 1 h in dark at 4 °C. Cells were further washed twice with sterile PBS by centrifuging at 650×g for 5 min at room temperature (~25 °C) to remove unbound antibodies and resuspended in sterile PBS before flow cytometric analysis.

Cell Viability Assay, Ex Vivo. Freshly isolated PBMCs from healthy individuals were seeded in 96-well plates (2×10^5 cells/well), treated with α-Mercurin at different concentrations, then incubated for 96 h. The 'no treatment' (NT) groups were treated with only media while "vehicle control" (VC) groups were treated with 1 mM NaOH solution. MTT reagent dissolved in water was added at the final concentration of 0.5 mg/mL and incubated for 4 h. Following incubation, the plates were centrifuged at 400×g for 15 min at 4 °C, protecting from light. The supernatant was exchanged with DMSO to dissolve the formazan crystals and absorbance was measured at 570 nm by TECAN Infinite M200 Pro microplate reader. The percent of the viable cells (% cell viability) was calculated considering the 'no treatment' (NT) group as 100% cell survival. All the representative graphs are prepared using Microsoft Excel software (n = 3, *$P < 0.05$; **$P < 0.01$; ***$P < 0.001$; Student's t test).

Cell viability or antiproliferative activity of the α-Mercurin was also investigated on PBMCs isolated from ALL patients, using flow cytometry. Freshly isolated PBMCs containing immature blasts from leukemia patients were seeded in 24-well plates (3×10^5 cells/well) and treated with 20 μM α-Mercurin for 72 h. The control groups were treated with only media. Cells were then harvested, and pellet was resuspended in 300 μL of sterile PBS containing 5% FBS. Scattering patterns (FSC-A/SSC-A) of the lymphocytes and immature blasts present in the whole volume were recorded using a flow cytometer (BD FACS LSRFortessa). Percent of viability of different treatment groups was calculated considering viability of the 'no treatment' group as 100%.

https://doi.org/10.1021/acsomega.4c10710
ACS Omega 2025, 10, 17416−17434

Blood Compatibility Assay, Ex Vivo. The whole blood samples from healthy individuals and acute leukemia patients were collected in K2-EDTA tubes. Further, the samples were divided and treated with 1× RBC lysis buffer, saline (0.9% NaCl), 20 μM α-Mercurin, and 1 mM NaOH solution, followed by incubation for 20 min at 37 °C. Following incubation, the samples were centrifuged at 1300xg for 10 min at room temperature. UV−visible spectra of the supernatants were recorded.

Mitochondrial Transmembrane Potential Assay, Ex Vivo. Freshly isolated PBMCs from leukemia patients were seeded in 24-well plates (3×10^5 cells/well) and treated with 20 μM α-Mercurin for 72 h. In case of the positive control group, cells were pretreated with a pseudodecoupler, picric acid. Then, 20 μM JC-1 dye dissolved in DMSO was added to each well and incubated for 20 min at 37 °C under 5% CO_2 and 95% air in a humidified atmosphere. Cells were further centrifuged at 400×g for 5 min at room temperature (∼25 °C) and pellets were resuspended in cold sterile PBS. Flow cytometric analysis was performed using BD LSRFortessa flow cytometer; JC-1_{red} (λ_{ex} = 543 nm, λ_{em} = 575−610 nm), JC-1_{green} (λ_{ex} = 488 nm, λ_{em} = 515−530 nm). All the analysis was performed using FlowJo V10.8.1.

Immunogenic Marker Expression Analysis, Ex Vivo. Role of the synthesized α-Mercurin on immunomodulation was analyzed by treating the PBMCs isolated from acute leukemia patients' (ALL) blood samples. Freshly isolated PBMCs were seeded in 24-well plates (3×10^5 cells/well) and treated with 20 μM α-Mercurin for 72 h. Thereafter, cells were washed twice with cold sterile PBS by centrifuging at 650xg using a REMI R8C centrifuge at room temperature (∼25 °C). Then, cells were stained with primary antibodies and incubated for 30 min in dark, keeping on ice. Cells were further washed two times with cold sterile PBS by centrifuging at 650xg using a REMI R8C centrifuge at room temperature (∼25 °C) to remove excess primary antibodies. Cells were then stained with FITC-tagged secondary antibodies and again incubated for 20 min in dark keeping on ice. Following incubation, cells were washed two times with cold sterile PBS by centrifuging at 650xg using a REMI R8C centrifuge at room temperature (∼25 °C) and resuspended in sterile PBS, containing 2.5% FBS before flow cytometric analysis.

Investigation of Subacute Toxicity, In Vivo. For the subacute toxicity study, eight healthy Swiss albino male mice, aged 4−5 weeks, weighing between 25 and 30 g were used. The animal experiment was performed following an approved protocol from the Institutional Ethics Committee for Animals (IECA) of the Chittaranjan National Cancer Institute (CNCI), Kolkata, India. All animals were supplied and housed by the CNCI animal facility. Housing was done in polypropylene cages (30 × 19 × 13 cm), with a stainless-steel wire cover, with four animals per cage and kept at room temperature (24 ± 2 °C) maintaining a light/dark cycle every 12 h. Two groups were established with 4 animals in each. Four animals in the treatment group were administered 80 μL α-Mercurin from a 2 mM stock (3.3 mg/kg body weight), intravenously, via the lateral tail vein, twice a week for 8 weeks, while control group animals were injected with an equal volume of sterile saline, following the same procedure. Throughout the 56-day study, all animals were observed daily for general health and any symptoms of toxicity, while body weights were recorded on days; 0, 3, 7, 10, 14, 17, 21, 24, 28, 31, 35, 38, 42, 45, 49, 52, and 56 of the experiment. At the end of the study, all animals were kept fasting overnight before blood sampling, followed by sacrifice.

Statistical Analysis. The statistical details, including performed statistical analysis, statistical significance thresholds/values, and, in most cases, the counts/number of data points are reported in the figure legends, figures, and/or materials and methods. All statistical analyses were performed using Microsoft Excel software. Statistical significance was calculated by Student's *t*-test. Details about the software used for analysis can also be found in the method section.

Human Studies: Ethics Statement. All experiments with human samples were conducted under the protocol approved by the Institutional Ethics Committee (IEC) of the Chittaranjan National Cancer Institute (CNCI), vide certificate number CNCI-IEC-SG-2020-17, dated 18/06/2020. Informed consent of all participating patients, along with the signed agreement from patients or their next of kin, were obtained before blood sampling (Consent form for 18 years and above, Assent form for 12−18 years, Child Verbal & Parental Consent form for 7−12 years and Parental Consent form for below 7 years). Blood samples were collected before initiation of any clinical treatment. Any ALL patient undergoing treatment was excluded from the study.

Animal Studies: Ethics Statement. All animal procedures are in accordance with the Institutional Animal Ethics Committee (IAEC) of the Chittaranjan National Institute (CNCI), Kolkata, India, and approved by the Committee for Control and Supervision of Experiments on Animals (CCSEA), vide certificate no. IAEC-1.1/2024/AH-12, dated March 13, 2024.

■ ASSOCIATED CONTENT

Supporting Information

The Supporting Information is available free of charge at https://pubs.acs.org/doi/10.1021/acsomega.4c10710.

Additional figures illustrating detailed biophysical characterization, in vitro, ex vivo, and in vivo studies, along with in silico analysis (PDF)

In vivo study demonstrating the behavioral pattern of control amimals (MP4)

In vivo study demonstrating the behavioral pattern of treated amimals (MP4)

■ AUTHOR INFORMATION

Corresponding Author

Supratim Ghosh − *Department of Anti-Cancer Drug Development and Chemotherapy, Chittaranjan National Cancer Institute, Kolkata 700026 West Bengal, India;* orcid.org/0000-0003-1552-0538; Email: supratimghosh@cnci.ac.in

Authors

Sougata Mondal − *Department of Anti-Cancer Drug Development and Chemotherapy, Chittaranjan National Cancer Institute, Kolkata 700026 West Bengal, India*

Upasana Das − *Department of Cancer Biology and Comprehensive Cancer Center, Wake Forest University School of Medicine, USA, Winston Salem, North Carolina 27157, United States*

Oyendrila Ghosh − *Department of Anti-Cancer Drug Development and Chemotherapy, Chittaranjan National Cancer Institute, Kolkata 700026 West Bengal, India*

https://doi.org/10.1021/acsomega.4c10710
ACS Omega 2025, 10, 17416−17434

Bidisha Maiti − *Department of Anti-Cancer Drug Development and Chemotherapy, Chittaranjan National Cancer Institute, Kolkata 700026 West Bengal, India*
Shuvam Halder − *Department of Medical Oncology, Chittaranjan National Cancer Institute, Kolkata 700026 West Bengal, India*
Uttam Pal − *Technical Research Centre, S.N. Bose National Centre for Basic Sciences, Kolkata 700106 West Bengal, India;* orcid.org/0000-0003-2110-4610
Kalyan Kusum Mukherjee − *Department of Medical Oncology, Chittaranjan National Cancer Institute, Kolkata 700026 West Bengal, India*

Complete contact information is available at: https://pubs.acs.org/10.1021/acsomega.4c10710

Author Contributions

#S.M. and U.D. are joint first authors for the article. S.M. and U.D. contributed equally to this work. The manuscript was written through contributions of all authors and all authors have given approval to the final version of the manuscript.

Funding

This project has received funding from the Indian Council of Medical Research (ICMR) via grant no. ICMR/AdHOC/2020-2532 and the Chittaranjan National Cancer Institute (CNCI) via intramural grant.

Notes

The authors declare the following competing financial interest(s): The present study is a part of the Indian patent application no. 202331041707 and PCT application no PCT/IN2024/050890, filed by the corresponding author, Supratim Ghosh. Other authors declare no conflict of interest.

■ ACKNOWLEDGMENTS

Authors acknowledge funding support from ICMR and CNCI. Authors also acknowledge Central Instrumentation Facility (CIF) of CSIR-IICB for supporting with their NMR facility along with FT-IR and Mass Spectrometry. Authors also acknowledge IACS, Kolkata and IIT-Patna for helping with their NMR facilities. Central Research Facility (CRF) of IIT Kharagpur is also acknowledged for assistance with X-ray Photoelectron Spectroscopy and Mass Spectrometry. Authors are thankful to the Bose Institute and S. N. Bose National Centre for Basic Sciences for supporting with Mass Spectrometry and EDAX analysis, respectively. Authors acknowledge NCCS, Pune, India as well for providing the cell lines.

■ REFERENCES

(1) Bhosale, P. B.; Ha, S. E.; Vetrivel, P.; Kim, H. H.; Kim, S. M.; Kim, G. S. Functions of Polyphenols and Its Anticancer Properties in Biomedical Research: A Narrative Review. *Transl. Cancer Res.* **2020**, *9* (12), 7619−7631.
(2) Nan, Y.; Su, H.; Zhou, B.; Liu, S. The Function of Natural Compounds in Important Anticancer Mechanisms. *Front. Oncol.* **2023**, *12*, No. 1049888.
(3) Casini, A.; Pöthig, A. Metals in Cancer Research: Beyond Platinum Metallodrugs. *ACS Cent. Sci.* **2024**, *10* (2), 242−250.
(4) Valente, A.; Podolski-Renić, A.; Poetsch, I.; Filipović, N.; López, Ó.; Turel, I.; Heffeter, P. Metal- and Metalloid-Based Compounds to Target and Reverse Cancer Multidrug Resistance. *Drug Resist. Updat.* **2021**, *58*, No. 100778.
(5) Siviero, A.; Gallo, E.; Maggini, V.; Gori, L.; Mugelli, A.; Firenzuoli, F.; Vannacci, A. Curcumin, a Golden Spice with a Low Bioavailability. *J. Herb. Med.* **2015**, *5* (2), 57−70.
(6) Dei Cas, M.; Ghidoni, R. Dietary Curcumin: Correlation between Bioavailability and Health Potential. *Nutrients* **2019**, *11* (9), 2147.
(7) Bernhoft, R. A. Mercury Toxicity and Treatment: A Review of the Literature. *J. Environ. Public Health* **2012**, *2012*, No. 460508.
(8) Wu, Y.-S.; Osman, A. I.; Hosny, M.; Elgarahy, A. M.; Eltaweil, A. S.; Rooney, D. W.; Chen, Z.; Rahim, N. S.; Sekar, M.; Gopinath, S. C. B.; Mat Rani, N. N. I.; Batumalaie, K.; Yap, P.-S. The Toxicity of Mercury and Its Chemical Compounds: Molecular Mechanisms and Environmental and Human Health Implications: A Comprehensive Review. *ACS Omega* **2024**, *9* (5), 5100−5126.
(9) Yuandani; Jantan, I.; Rohani, A. S.; Sumantri, I. B. Immunomodulatory Effects and Mechanisms of Curcuma Species and Their Bioactive Compounds: A Review. *Front. Pharmacol.* **2021**, *12*. .
(10) Gautam, S. C.; Gao, X.; Dulchavsky, S. Immunomodulation by Curcumin. *Adv. Exp. Med. Biol.* **2007**, *595*, 321−341.
(11) Srivastava, R. M.; Singh, S.; Dubey, S. K.; Misra, K.; Khar, A. Immunomodulatory and Therapeutic Activity of Curcumin. *Int. Immunopharmacol.* **2011**, *11* (3), 331−341.
(12) Tomeh, M. A.; Hadianamrei, R.; Zhao, X. A Review of Curcumin and Its Derivatives as Anticancer Agents. *Int. J. Mol. Sci.* **2019**, *20* (5), 1033.
(13) Wilken, R.; Veena, M. S.; Wang, M. B.; Srivatsan, E. S. Curcumin: A Review of Anti-Cancer Properties and Therapeutic Activity in Head and Neck Squamous Cell Carcinoma. *Mol. Cancer* **2011**, *10* (1), 12.
(14) Zoi, V.; Galani, V.; Lianos, G. D.; Voulgaris, S.; Kyritsis, A. P.; Alexiou, G. A. The Role of Curcumin in Cancer Treatment. *Biomedicines* **2021**, *9* (9), 1086.
(15) Kouhpeikar, H.; Butler, A. E.; Bamian, F.; Barreto, G. E.; Majeed, M.; Sahebkar, A. Curcumin as a Therapeutic Agent in Leukemia. *J. Cell. Physiol.* **2019**, *234* (8), 12404−12414.
(16) Yu, J.; Peng, Y.; Wu, L.-C.; Xie, Z.; Deng, Y.; Hughes, T.; He, S.; Mo, X.; Chiu, M.; Wang, Q.-E.; He, X.; Liu, S.; Grever, M. R.; Chan, K. K.; Liu, Z. Curcumin Down-Regulates DNA Methyltransferase 1 and Plays an Anti-Leukemic Role in Acute Myeloid Leukemia. *PloS One* **2013**, *8* (2), No. e55934.
(17) Kuttikrishnan, S.; Siveen, K. S.; Prabhu, K. S.; Khan, A. Q.; Ahmed, E. I.; Akhtar, S.; Ali, T. A.; Merhi, M.; Dermime, S.; Steinhoff, M.; Uddin, S. Curcumin Induces Apoptotic Cell Death via Inhibition of PI3-Kinase/AKT Pathway in B-Precursor Acute Lymphoblastic Leukemia. *Front. Oncol.* **2019**, *9*, 484.
(18) Anand, P.; Kunnumakkara, A. B.; Newman, R. A.; Aggarwal, B. B. Bioavailability of Curcumin: Problems and Promises. *Mol. Pharmaceutics* **2007**, *4* (6), 807−818.
(19) Yang, K.-Y.; Lin, L.-C.; Tseng, T.-Y.; Wang, S.-C.; Tsai, T.-H. Oral Bioavailability of Curcumin in Rat and the Herbal Analysis from Curcuma Longa by LC-MS/MS. *J. Chromatogr. B Analyt. Technol. Biomed. Life. Sci.* **2007**, *853* (1−2), 183−189.
(20) Wang, Y.-J.; Pan, M.-H.; Cheng, A.-L.; Lin, L.-I.; Ho, Y.-S.; Hsieh, C.-Y.; Lin, J.-K. Stability of Curcumin in Buffer Solutions and Characterization of Its Degradation Products. *J. Pharm. Biomed. Anal.* **1997**, *15* (12), 1867−1876.
(21) Vyas, A.; Dandawate, P.; Padhye, S.; Ahmad, A.; Sarkar, F. Perspectives on New Synthetic Curcumin Analogs and Their Potential Anticancer Properties. *Curr. Pharm. Des.* **2013**, *19* (11), 2047−2069.
(22) Mbese, Z.; Khwaza, V.; Aderibigbe, B. A. Curcumin and Its Derivatives as Potential Therapeutic Agents in Prostate, Colon and Breast Cancers. *Molecules* **2019**, *24* (23), 4386.
(23) Adeluola, A.; Zulfiker, A. H. M.; Brazeau, D.; Amin, A. R. M. R. Perspectives for Synthetic Curcumins in Chemoprevention and Treatment of Cancer: An Update with Promising Analogues. *Eur. J. Pharmacol.* **2021**, *906*, No. 174266.

(24) Ghosh, S.; Mallick, S.; Das, U.; Verma, A.; Pal, U.; Chatterjee, S.; Nandy, A.; Saha, K. D.; Maiti, N. C.; Baishya, B.; Suresh Kumar, G.; Gmeiner, W. H. Curcumin Stably Interacts with DNA Hairpin through Minor Groove Binding and Demonstrates Enhanced Cytotoxicity in Combination with FdU Nucleotides. *Biochim. Biophys. Acta BBA - Gen. Subj.* **2018**, *1862* (3), 485−494.
(25) Mundekkad, D.; Cho, W. C. Applications of Curcumin and Its Nanoforms in the Treatment of Cancer. *Pharmaceutics* **2023**, *15* (9), 2223.
(26) Karthikeyan, A.; Senthil, N.; Min, T. Nanocurcumin: A Promising Candidate for Therapeutic Applications. *Front. Pharmacol.* **2020**, *11*, 487.
(27) Prasad, S.; DuBourdieu, D.; Srivastava, A.; Kumar, P.; Lall, R. Metal−Curcumin Complexes in Therapeutics: An Approach to Enhance Pharmacological Effects of Curcumin. *Int. J. Mol. Sci.* **2021**, *22* (13), 7094.
(28) Wanninger, S.; Lorenz, V.; Subhan, A.; Edelmann, F. T. Metal Complexes of Curcumin−Synthetic Strategies, Structures and Medicinal Applications. *Chem. Soc. Rev.* **2015**, *44* (15), 4986−5002.
(29) Das, U.; Bhuniya, A.; Roy, A. K.; Gmeiner, W. H.; Ghosh, S. Hairpin Oligonucleotide Can Functionalize Gold Nanorods for in Vivo Application Delivering Cytotoxic Nucleotides and Curcumin: A Comprehensive Study in Combination with Near-Infrared Laser. *ACS Omega* **2020**, *5* (44), 28463−28474.
(30) Song, Y.-M.; Xu, J.-P.; Ding, L.; Hou, Q.; Liu, J.-W.; Zhu, Z.-L. Syntheses, Characterization and Biological Activities of Rare Earth Metal Complexes with Curcumin and 1,10-Phenanthroline-5,6-Dione. *J. Inorg. Biochem.* **2009**, *103* (3), 396−400.
(31) Mohammadi, K.; Thompson, K. H.; Patrick, B. O.; Storr, T.; Martins, C.; Polishchuk, E.; Yuen, V. G.; McNeill, J. H.; Orvig, C. Synthesis and Characterization of Dual Function Vanadyl, Gallium and Indium Curcumin Complexes for Medicinal Applications. *J. Inorg. Biochem.* **2005**, *99* (11), 2217.
(32) Valentini, A.; Conforti, F.; Crispini, A.; De Martino, A.; Condello, R.; Stellitano, C.; Rotilio, G.; Ghedini, M.; Federici, G.; Bernardini, S.; Pucci, D. Synthesis, Oxidant Properties, and Antitumoral Effects of a Heteroleptic Palladium(II) Complex of Curcumin on Human Prostate Cancer Cells. *J. Med. Chem.* **2009**, *52* (2), 484−491.
(33) Zambre, A. P.; Kulkarni, V. M.; Padhye, S.; Sandur, S. K.; Aggarwal, B. B. Novel Curcumin Analogs Targeting TNF-Induced NF-κB Activation and Proliferation in Human Leukemic KBM-5 Cells. *Bioorg. Med. Chem.* **2006**, *14* (21), 7196−7204.
(34) Zhang, N.; Wu, J.; Wang, Q.; Liang, Y.; Li, X.; Chen, G.; Ma, L.; Liu, X.; Zhou, F. Global Burden of Hematologic Malignancies and Evolution Patterns over the Past 30 Years. *Blood Cancer J.* **2023**, *13* (1), 82.
(35) Huang, J.; Chan, S. C.; Ngai, C. H.; Lok, V.; Zhang, L.; Lucero-Prisno, D. E.; Xu, W.; Zheng, Z.-J.; Elcarte, E.; Withers, M.; Wong, M. C. S. Disease Burden, Risk Factors, and Trends of Leukaemia: A Global Analysis. *Front. Oncol.* **2022**, *12*, No. 904292.
(36) Shi, Y.; Chen, C.; Huang, Y.; Xu, Y.; Xu, D.; Shen, H.; Ye, X.; Jin, J.; Tong, H.; Yu, Y.; Tang, X.; Li, A.; Cui, D.; Xie, W. Global Disease Burden and Trends of Leukemia Attributable to Occupational Risk from 1990 to 2019: An Observational Trend Study. *Front. Public Health* **2022**, *10*. .
(37) Miranda-Filho, A.; Piñeros, M.; Ferlay, J.; Soerjomataram, I.; Monnereau, A.; Bray, F. Epidemiological Patterns of Leukaemia in 184 Countries: A Population-Based Study. *Lancet Haematol.* **2018**, *5* (1), e14−e24.
(38) Du, M.; Chen, W.; Liu, K.; Wang, L.; Hu, Y.; Mao, Y.; Sun, X.; Luo, Y.; Shi, J.; Shao, K.; Huang, H.; Ye, D. The Global Burden of Leukemia and Its Attributable Factors in 204 Countries and Territories: Findings from the Global Burden of Disease 2019 Study and Projections to 2030. *J. Oncol.* **2022**, *2022*, No. 1612702.
(39) Stentoft, J. The Toxicity of Cytarabine. *Drug Saf.* **1990**, *5* (1), 7−27.
(40) Barrios, N. J.; Tebbi, C. K.; Freeman, A. I.; Brecher, M. L. Toxicity of High Dose Ara-C in Children and Adolescents. *Cancer* **1987**, *60* (2), 165−169.
(41) Di Francia, R.; Crisci, S.; De Monaco, A.; Cafiero, C.; Re, A.; Iaccarino, G.; De Filippi, R.; Frigeri, F.; Corazzelli, G.; Micera, A.; Pinto, A. Response and Toxicity to Cytarabine Therapy in Leukemia and Lymphoma: From Dose Puzzle to Pharmacogenomic Biomarkers. *Cancers* **2021**, *13* (5), 966.
(42) Cienkusz, M.; Drabko, K. The Incidence and Clinical Spectrum of Vincristine- Induced Peripheral Neuropathy in Patients with Acute Lymphoblastic Leukemia- a Prospective Study of Twenty-Nine Cases. *Acta Haematol. Polym.* **2024**, *55* (1), 42−47.
(43) Yu, H.; Qiu, Y.; Yu, H.; Wang, Z.; Xu, J.; Peng, Y.; Wan, X.; Wu, X.; Jin, R.; Zhou, F. Anthracycline Induced Cardiac Disorders in Childhood Acute Lymphoblastic Leukemia: A Single-Centre, Retrospective, Observational Study. *Front. Pharmacol.* **2021**, *12*. .
(44) Fu, S. H.; Flannery, A. H.; Thompson Bastin, M. L. Acute Hepatotoxicity After High-Dose Cytarabine for the Treatment of Relapsed Acute Myeloid Leukemia: A Case Report. *Hosp. Pharm.* **2019**, *54* (3), 160−164.
(45) Garg, G.; Chawla, N.; Gogia, A.; Kakar, A. Low Backache in Adults as an Initial Presentation of Acute Lymphoblastic Leukemia. *J. Fam. Med. Prim. Care* **2017**, *6* (2), 434−436.
(46) Franz, K. J.; Metzler-Nolte, N. Introduction: Metals in Medicine. *Chem. Rev.* **2019**, *119* (2), 727−729.
(47) Ravishankar, B.; Shukla, V. Indian Systems of Medicine: A Brief Profile. *Afr. J. Tradit. Complement. Altern. Med.* **2008**, *4* (3), 319−337.
(48) *Vaccines and immunization: Thiomersal*. https://www.who.int/news-room/questions-and-answers/item/vaccines-and-immunization-thiomersal (accessed 2024-09-02).
(49) Pichichero, M. E.; Cernichiari, E.; Lopreiato, J.; Treanor, J. Mercury Concentrations and Metabolism in Infants Receiving Vaccines Containing Thiomersal: A Descriptive Study. *Lancet* **2002**, *360* (9347), 1737−1741.
(50) Thas, J. J. Siddha Medicine—Background and Principles and the Application for Skin Diseases. *Clin. Dermatol.* **2008**, *26* (1), 62−78.
(51) Arunachalam, J. Researches on Mercurial Preparations: The Prime Requirement for Their Acceptance in Medical World. *Ayu* **2015**, *36* (2), 118−124.
(52) Yadav, K. D.; Chaudhary, A. K. Classical and Contemporary Methods for Conversion of Toxic Unstable Mercury to Safe and Stable Mercury. *Ind. J. Tradit. Knowl.* **2016**, *15*, 514.
(53) Kannan, N.; Shanmuga Sundar, S.; Balaji, S.; Amuthan, A.; Anil Kumar, N. V.; Balasubramanian, N. Physiochemical Characterization and Cytotoxicity Evaluation of Mercury-Based Formulation for the Development of Anticancer Therapeuticals. *PloS One* **2018**, *13* (4), No. e0195800.
(54) Li, Q.; Yang, Z.; Zhang, P.; Zhao, Y.; Yu, X.; Xue, P.; Shao, Y.; Li, Q.; Jia, X.; Zhang, Q.; Cheng, L.; He, M.; Zhou, Z.; Zhang, Y. Mercury Impact on Hematopoietic Stem Cells Is Regulated by IFNγ-Dependent Bone Marrow-Resident Macrophages in Mice. *Toxicol. Lett.* **2018**, *295*, 54−63.
(55) *Mercury and Health*. https://www.who.int/news-room/fact-sheets/detail/mercury-and-health (accessed 2024-08-28).
(56) Perera, K. D. C.; Weragoda, G. K.; Haputhanthri, R.; Rodrigo, S. K. Study of Concentration Dependent Curcumin Interaction with Serum Biomolecules Using ATR-FTIR Spectroscopy Combined with Principal Component Analysis (PCA) and Partial Least Square Regression (PLS-R). *Vib. Spectrosc.* **2021**, *116*, No. 103288.
(57) Cecconi, F.; Ghilardi, C. A.; Midollini, S.; Orlandini, A.; Vacca, A. Synthesis, Characterization and X-Ray Structure of the Organomercurial Complex [Hg(C6F5)(Np3)](CF3SO3), np3 = N-(CH2CH2PPh2)3. *Polyhedron* **2001**, *20* (22−23), 2885−2888.
(58) Borovik, A. S.; Bott, S. G.; Barron, A. R. Hydrogen/Deuterium Exchange Catalyzed by an Unusually Stable Mercury−Toluene Complex. *Angew. Chem.* **2000**, *112* (22), 4283−4284.

(59) Kuz'mina, L. G.; Bokii, N.; Struchkov, Y. T. The Structural Chemistry of Organic Compounds of Mercury and Its Analogues (Zinc and Cadmium). *Russ. Chem. Rev.* **1975**, *44* (1), 73.
(60) Ahmed, M.; Abdul Qadir, M.; Imtiaz Shafiq, M.; Muddassar, M.; Hameed, A.; Nadeem Arshad, M.; Asiri, A. M. Curcumin: Synthesis Optimization and *in Silico* Interaction with Cyclin Dependent Kinase. *Acta Pharm.* **2017**, *67* (3), 385−395.
(61) Prasad, C.; Bhatia, E.; Banerjee, R. Curcumin Encapsulated Lecithin Nanoemulsions: An Oral Platform for Ultrasound Mediated Spatiotemporal Delivery of Curcumin to the Tumor. *Sci. Rep.* **2020**, *10* (1), 8587.
(62) Dai, Y.; Terskikh, V.; Brinmkmann, A.; Wu, G. Solid-State ^{1}H, ^{13}C, and ^{17}O NMR Characterization of the Two Uncommon Polymorphs of Curcumin. *Cryst. Growth Des.* **2020**, *20* (11), 7484−7491.
(63) Kong, X.; Brinkmann, A.; Terskikh, V.; Wasylishen, R. E.; Bernard, G. M.; Duan, Z.; Wu, Q.; Wu, G. Proton Probability Distribution in the O···H···O Low-Barrier Hydrogen Bond: A Combined Solid-State NMR and Quantum Chemical Computational Study of Dibenzoylmethane and Curcumin. *J. Phys. Chem. B* **2016**, *120* (45), 11692−11704.
(64) Kavitha, N.; Anantha Lakshmi, P. V. Synthesis, Characterization and Thermogravimetric Analysis of Co(II), Ni(II), Cu(II) and Zn(II) Complexes Supported by ONNO Tetradentate Schiff Base Ligand Derived from Hydrazino Benzoxazine. *J. Saudi Chem. Soc.* **2017**, *21*, S457−S466.
(65) Singh, A. K.; Yadav, S.; Sharma, K.; Firdaus, Z.; Aditi, P.; Neogi, K.; Bansal, M.; Gupta, M. K.; Shanker, A.; Singh, R. K.; Prakash, P. Quantum Curcumin Mediated Inhibition of Gingipains and Mixed-Biofilm of *Porphyromonas Gingivalis* Causing Chronic Periodontitis. *RSC Adv.* **2018**, *8* (70), 40426−40445.
(66) Reddy, I.; Mallikarjuna, K.; Ghfar, A.; Rosaiah, P.; Akkinepally, B.; Dhanasekar, M.; Shim, J.; Bai, C. Photoelectrochemical Charge Kinetics and Transfer Mechanisms of Organic Curcumin (Turmeric) Photoelectrodes. *J. Appl. Electrochem.* **2024**, *54*, 2637.
(67) Humbert, P. An XPS and UPS Photoemission Study of HgO. *Solid State Commun.* **1986**, *60* (1), 21−24.
(68) Glans, P.-A.; Learmonth, T.; Smith, K. E.; Guo, J.; Walsh, A.; Watson, G. W.; Terzi, F.; Egdell, R. G. Experimental and Theoretical Study of the Electronic Structure of HgO and Tl_2O_3. *Phys. Rev. B* **2005**, *71* (23), No. 235109.
(69) Saper, R. B.; Kales, S. N.; Paquin, J.; Burns, M. J.; Eisenberg, D. M.; Davis, R. B.; Phillips, R. S. Heavy Metal Content of Ayurvedic Herbal Medicine Products. *JAMA* **2004**, *292* (23), 2868−2873.
(70) Gogtay, N. J.; Bhatt, H. A.; Dalvi, S. S.; Kshirsagar, N. A. The Use and Safety of Non-Allopathic Indian Medicines. *Drug Saf.* **2002**, *25* (14), 1005−1019.
(71) Zhao, M.; Li, Y.; Wang, Z. Mercury and Mercury-Containing Preparations: History of Use, Clinical Applications, Pharmacology, Toxicology, and Pharmacokinetics in Traditional Chinese Medicine. *Front. Pharmacol.* **2022**, *13*, No. 807807.
(72) Liu, Y.-M.; Liu, B.; Liu, J.; Xu, S.-F.; Zhang, F.; Cheng, M.-L.; Shi, J.-S. Cinnabar-Containing Chinese Medicine Hua-Feng-Dan Differs from Mercury Sulfide and Mercury Chloride in Affecting Gut Microbiota in Mice. *Pharmacol. Res. - Mod. Chin. Med.* **2023**, *8*, No. 100279.
(73) Peng, C.; Kang, L.; Yuan, X.; Qiao, J.; Fan, Y.; Yao, L.; Qi, K.; Sun, Y.; Dai, X.; Zhang, Y.; Huo, Q. Research Progress in the Analysis of Chemical Forms of Mercury in Traditional Chinese Medicine. *Processes* **2023**, *11* (10), 2821.
(74) *G09 | Gaussian.com*. https://gaussian.com/glossary/g09/ (accessed 2024-08-27).
(75) Zhao, Y.; Truhlar, D. G. A New Local Density Functional for Main-Group Thermochemistry, Transition Metal Bonding, Thermochemical Kinetics, and Noncovalent Interactions. *J. Chem. Phys.* **2006**, *125* (19), 194101.
(76) Marenich, A. V.; Cramer, C. J.; Truhlar, D. G. Universal Solvation Model Based on Solute Electron Density and on a Continuum Model of the Solvent Defined by the Bulk Dielectric Constant and Atomic Surface Tensions. *J. Phys. Chem. B* **2009**, *113* (18), 6378−6396.

https://doi.org/10.1021/acsomega.4c10710
ACS Omega 2025, 10, 17416−17434